Micromachined Differential Scanning Calorimeter for Cellular Differentiation and Metabolism Monitoring

Robert Blise
Marquette University

MICROMACHINED DIFFERENTIAL SCANNING CALORIMETER FOR CELLULAR DIFFERENTIATION AND METABOLISM MONITORING

by

Robert J. Blise, B.S.

A Thesis submitted to the Faculty of the Graduate School,
Marquette University
in Partial Fulfillment of the Requirements for
the Degree of Master of Science

Milwaukee, Wisconsin

May 2011

ABSTRACT
MICROMACHINED DIFFERENTIAL SCANNING CALORIMETER FOR CELLULAR DIFFERENTIATION AND METABOLISM MONITORING

Robert J. Blise, B.S.

Marquette University, 2011

This thesis presents a micromachined differential scanning calorimeter (DSC) for cellular differentiation and metabolism monitoring. The misregulation of cell physiology due to disease increases the metabolic rate of the cell and therefore its heat output. Observing or monitoring the cell's heat output will lead to a method to detect diseased cells and distinguish them from normal cells.

The calorimetric chambers of the DSC were fabricated on a silicon nitride thin film, which allows for rapid thermal equilibrium and insulation. The temperature sensing element was a resistive temperature detector fabricated from nickel. The DSC incorporated integrated nickel resistive heaters to apply on chip heating and for calibration.

The cell metabolism experiments carried out with the DSC were performed using JM-1 liver cancer cells and white blood cells (lymphocytes). Step voltage inputs were applied to the DSC while the response of the RTD to temperature was monitored. The results from initial testing showed a detectable increase in chamber temperature of 0.375ºC for the JM-1 liver cells. Further analysis was completed by obtaining the derivative of the DSC temperature curves. Two methods were explored: the direct derivative of the raw data curve and the derivative of the differential data curve. While both methods showed the ability to differentiate between the JM-1 liver cells and the lymphocytes, the derivative of the differential data curve was superior due to the elimination of common mode signals. The differential method also allowed the determination of the heat rates of the cells. JM-1 liver cells showed a positive heat rate which is consistent with its increased metabolism, while the lymphocytes showed a negative heat rate or absorption of thermal energy.

ACKNOWLEDGMENTS

Robert J. Blise, B.S.

There are several people I would like to acknowledge for their support during my thesis work. First I would like to thank my advisor, Dr. Chung Hoon Lee, for his patience while I took on this project as well as for his guidance, insight, and discussions during the course of the past few years. I would also like to thank Dr. Fabien Josse and Dr. Susan Schneider for their suggestions and comments to improve my work throughout its progression and for being part of my committee.

I would especially like to thank my fiancé, Rachel, for her unending support and motivation. She has always been positive through the past seven years while I went back to school to achieve all that I would have not been able to do without her. I will be forever grateful to you for what you have done and sacrificed.

I would also like to thank my parents for the confidence they had in me when mine seemed to be low. I would like to thank my friends for being there when my family could not be. Further I would like to thank Jun Hyun Han for his help in the lab with fabrication and with discussions regarding my work.

TABLE OF CONTENTS

LIST OF TABLES

LIST OF FIGURES

1 Introduction

The goal of this thesis work is to observe and measure the heat generated by the metabolism of biological cells using a micromachined calorimeter. By observing the cells' metabolic rate, it will be possible to distinguish between abnormal and normal cells. Micro-calorimetry is a very useful technique in the biological sciences for the study of the energy generation of complex biological processes such as protein-protein interactions, enzyme kinetics, and cell metabolism[1-3]. Current approaches to cell-based analysis tend to focus on the development of specific assays, which requires an understanding of the complex signaling molecules and cellular pathways[2]. Changes in the temperature of cells provide a measure of altered cellular metabolism that is not stimulus specific. However, it is an extremely difficult task to measure thermal signals from small numbers of living cells both because of their low thermal activity level and because of the challenge to maintain the viability of the cells[3]. By using established silicon processing techniques developed for the integrated circuit industry; one can produce micro-calorimetric devices that have very small sample chambers, which allow the use of nano- or picoliter volumes. These devices can achieve excellent thermal isolation by using nitride based membranes as support structures and very sensitive sensors through thin film resistive temperature detectors (RTD) or thermocouples.

Similar micro-calorimetric systems have been developed. Joannessen et al. have been able to test a low number of cells and observe the temperature changes and heat power output changes of several cell types after exposing them to noradrenaline[4]. Verhaegen et al. also developed a device capable of measuring cellular activity. They

were able to observe the baseline metabolism and the increase in metabolism due to the addition of oxytocin hormones[5]. Most of the existing micro-calorimeters are single reaction chamber systems, which are subjected to noise from the environment.

Our micro-calorimetric device was fabricated from silicon and configured as a differential scanning calorimeter (DSC). This configuration utilizes twin chambers, a sample and a reference chamber. The DSC method has the advantage of eliminating common mode noise fluctuations such as changes in room temperature. The thermal sensors were thin film nickel RTD's with integrated nickel heaters for supplying specific amounts of heat and for calibration. The sensors and heaters were patterned on a thin nitride film created by etching through a silicon wafer. The regularly etched pit served as the sample and reference chambers.

1.1 Cells

Cells are the fundamental building blocks of all forms of life[6]. The basic physiological functions of multi-cellular organisms reside in the cell[6]. These functions include absorption, evolution and transport of heat energy[7]. When alive and active, cells produce and consume energy as they function, grow and reproduce. Cells typically capture, store and then use this energy for their metabolic activities[7]. These actions are the basics of cellular metabolism. This metabolism has an associated heat or heat power output that is generated continuously by the cells. The metabolism of a cell and its heat output can be altered by the uptake of chemicals such as glucose or hormones, and more importantly, through the inception of diseases.

Diseases at the organism level, such as cancer, cause the misregulation of cellular physiology and therefore change the heat energy output and temperature of the cell[6]. By observing the temperature or heat power generation of populations of cells, it will be possible to study their metabolic activity, which could lead to the early detection of abnormal cells[4]. Simply observing the temperature of the potentially diseased cells versus a normal cell of the same type should lead to a means for early detection of diseases without the need to label or trigger the cells. This same approach can be applied to different cell types because two different cells may have different metabolic rates and therefore different heat outputs. Using this method will allow the ability to distinguish between cells solely based on their power outputs.

Cells are incredibly complex and diverse structures capable not only of self-replication, but also of performing a wide range of specialized tasks in multi-cellular organisms. The structure of the cell consists of a plasma membrane which houses specialized structures called organelles that generate energy, transport products, and contain deoxyribonucleic acid (DNA) as genetic material[8,9]. Cells are divided into two major categories by the presence or absence of a nuclear membrane that surrounds the DNA[8-10]. Prokaryotic cells such as bacteria, lack a nucleus, their genomes are less complex, and they do not contain cytoplasmic organelles or a cytoskeleton[8-10]. They are smaller and simpler with diameters ranging from 1μm to 10μm[8].

Eukaryotic cells contain ribosomes, a nucleus, a variety of cytoplasmic organelles, and a cytoskeleton. The largest and most prominent organelle of eukaryotic cells is the nucleus, with a diameter of 5μm[9]. Along with the nucleus, cells contain a variety of membrane-enclosed organelles within their cytoplasm[9,10]. These organelles

provide compartments in which different metabolic activities are localized. This compartmentalization provided by cytoplasmic organelles is what allows eukaryotic cells to function efficiently. Mitochondria, which are found in almost all eukaryotic cells, are the sites of oxidative metabolism and are thus responsible for generating most of the adenosine 5'-triphosphate (ATP) derived from the breakdown of organic molecules[9,10]. The endoplasmic reticulum and the Golgi apparatus are specifically devoted to the sorting and transport of proteins destined for secretion, incorporation into the plasma membrane, and incorporation into lysosomes[9,10]. The cytoskeleton is a network of protein filaments extending throughout the cytoplasm[9]. The cytoskeleton provides the structural framework of the cell, determining cell shape and the general organization of the cytoplasm[9]. It is also responsible for the movements of entire cells and for the intracellular transport and positioning of organelles and other structures[9,10].

1.2 Metabolism

All living things need energy to do work, such as maintain cell structure, function, grow, and reproduce[10]. The tasks that a cell must perform, such as movement and the synthesis of macromolecules, require energy[9]. A large portion of the cell's activities is therefore devoted to obtaining energy from the environment and using that energy to drive energy-requiring reactions[9]. Cells must constantly expend energy derived from the environment. The generation and utilization of metabolic energy is thus fundamental to all cell biology[9]. All cells use adenosine 5'-triphosphate (ATP) as their source of metabolic energy to drive the synthesis of cell constituents and carry out other energy requiring activities, such as movement[9].

1.3 Calorimetry

Whenever a sample of material is to be studied, one of the easiest tests to perform is to heat it. The observation of the behavior of the sample and the quantitative measurement of the changes in temperature can yield a great deal of useful information on the nature of the material[11]. Calorimetry is the measurement of heat. To measure heat is to exchange heat, and this exchange has to be conceived as coupled with an exchange of energy[12,13]. Heat is the amount of energy exchanged within a given time interval in the form of a heat flux[12]. The exchanged heat tends to effect a temperature change in a body that can be used as a measure of the heat exchanged13. Chemical reactions and physical transitions such as phase changes are connected with the generation or consumption of heat[13]. High sensitivity to temperature and signal stability over long periods of time makes calorimetry a universal method for investigating the heat changes which occur during such processes[11-13]. Calorimetric methods may be classified either by the principle of measurement, by the method of operation, or by the construction principle[11].

1.3.1 Measuring Principle

Heat conduction calorimeters operate at a constant temperature. The heat liberated from a reaction is entirely diluted within a heat sink. Modern isothermal calorimeters measure the conduction of heat as it travels between the reaction crucible and the surroundings. They often have a very high degree of sensitivity. Heat accumulation calorimeters allow a rise in temperature of the reaction system for exothermic reactions or a decrease in temperature for endothermic reactions. A reaction is monitored by measuring the temperature change as a function of time. Modern calorimeters allow the

signal to be converted into power. Heat exchange calorimeters actively exchange heat between the sample and the surroundings often during a temperature scanning experiment. The heat flow rate is determined by the temperature difference along the thermal resistance between the sample and surroundings.

1.3.2 Mode of Operation

Isothermal operation is when the sample and surroundings are held at a constant temperature ($\Delta T = 0, T_S = \text{constant}$)[14]. The surroundings and the chamber measuring system have the same constant temperature, i.e., the temperature of the furnace equals the temperature being measured[12].

Isoperibol operation refers to the use of a calorimeter at constant temperature of the surroundings with a possibly different temperature of the chamber measuring system[12]. In Isoperibol operation, the surroundings stay a constant temperature while the sample temperature may alter ($\Delta T \neq 0, T_E = \text{constant}$)[14]. Due the existence of a finite, defined thermal resistance, R_{th}, between the measuring system and the surroundings, the heat exchange depends in a definite manner on the sample chamber temperature and the furnace temperature only[12]. The temperature of the measuring system, T_M, changes by heat exchanged with the surroundings until equilibrium is established. This process necessitates a certain interval of time[12].

For adiabatic operation, ideally no heat exchange takes place between the sample and surroundings because they are both maintained at the same temperature, which may increase during the reaction ($\Delta T = 0, T_S \neq \text{constant}$)[14]. There are three ways of meeting this requirement: (1) The sample reaction takes place so rapidly that no appreciable

quantity of heat can leave or enter during the measuring interval; (2) the measuring system is separated from the surroundings by an "infinitely large" thermal resistance, i.e., thermally insulated in the best possible way; or (3) the temperature of the surroundings is so controlled as to be always equal to that of the measuring system, i.e., $T_F(t) = T_M(t)$ [14]. The advantage of the adiabatic method is most pronounced in the calorimetric investigation of reactions where heat is released at a slow or moderate rate[12].

1.3.3 Principle of Calorimeter Construction

The construction may have a single measuring system or a twin measuring system. Simple solution calorimeters have a single cell, while differential calorimeters have twin cells, a sample and reference. Two different applications of this configuration are possible depending upon the signal obtained from the experiment. Differential scanning calorimetry is the measurement of the change of the difference in the heat flow rate to the sample and to a reference sample while they are subjected to a controlled temperature program[13]. Differential thermometry is the measurement of the change of the difference in temperature between the sample and the reference sample while they are subjected to a controlled temperature program[13].

The term "differential" emphasizes an important feature of the technique—two identical temperature sensors are used, one for the sample and one for the reference, and the means of heating the sample and the reference are incorporated into the DSC cell[12,15]. The signal from the instrument depends on the difference between the responses of the two temperature sensors. A computer is used to operate the controls and provides a

method for data capture. The use of differential measurements reduces the effects of internal and external noise and transient fluctuations[12,15].

Most differential scanning calorimeters fall into one of two categories depending on their operating principle: power compensation or heat flux[12]. While operated in power compensation mode, the sample and reference are isolated from each other and have their own sensors and heaters. In the event of a temperature difference arising between the sample and reference, differential thermal power is supplied to the heaters to eliminate the difference and to maintain the temperature at the program value[14]. The differential thermal power is the source of the instrument signal[14].

In heat flux mode, the instrument signal is derived from the temperature difference established when the sample and reference are heated in the same furnace[14]. Both types of differential scanning calorimeters make use of crucibles to contain the sample and reference. The reference can be either an inert material in the crucible or simply the empty crucible. Crucibles commonly measure 5-6 mm in diameter, which gives some idea of the overall dimensions of the commercially available DSC cell.

Calorimetric measurements link thermal power to heat capacity, $d\Delta q/dt = (C_S - C_R)\beta$, and its integral, $\int (d\Delta q/dt)dt$, to energy or enthalpy[15]. Where the heat flux is q, C_S and C_R are the heat capacities of the sample and reference respectively, and β is the heating rate. These linkages together with measurements of temperature and determinations of phase changes form the basis of quantitative DSC[15]. Heat capacity is a key thermodynamic quantity because of its intrinsic importance and its relationship to other quantities such as enthalpy and entropy[12,14]. Specific heat capacity is

the amount of heat which a gram of a given substance has to exchange with its surroundings under certain conditions in order to change its temperature by one degree. Hence, a calorimeter used for the measurement of specific heat capacities contains a source of heat (usually electric), which delivers an exactly known heat flux into the sample, and a temperature measuring device, which determines the change in temperature of the sample[12]. The heat capacity is calculated from:

$$C = \frac{\Delta Q}{m\Delta T} \qquad (1.1)$$

where Q is the heat flux, m is the mass and T the resulting changes in the temperature of the sample[12,13].

The heat of reaction is the heat exchanged between a substance and its surroundings in the course of a chemical reaction. The spontaneous decomposition of a substance is usually associated with the release of heat to its surroundings. This heat can be measured by allowing the reaction to occur inside a container located within a body of known heat capacity. If the thermal insulation is such that the only exchange of heat takes place with the reacting substance, the heat of reaction may then be calculated from the measured temperature rise of the body. Integration of the heat flux over time yields the heat of reaction. The heat flux is proportional to the extent of the chemical reaction, which in turn may lead to certain conclusions about the reaction kinetics[12,13].

Calorimeters have even been used as biosensors to measure the heat produced by living organisms. Every organism is engaged in a constant exchange of heat with its surroundings. This heat flux results from metabolic processes may be traced by the heat fluxes measured in a calorimeter. A calorimeter built for this purpose must operate so that

the change to be measured is due entirely to an exchange of heat with nothing but the organism in the calorimeter[12,13].

1.4 Sensors

A sensor is a device that receives a quantity or energy and responds with a usable electrical signal output[16-18]. The output can be any form, ac or dc signal, change in resistance or capacitance, even analog or digital. It is determined by the sensor's electromechanical and/or chemical makeup[17]. The received quantity or energy that is sensed and converted is called the measurand[16,17]. The measurand can be one of or combinations of quantities: position, motion, sound, light, flow, force, radiation or temperature[16,17]. Sensors can be passive, meaning they do not need any additional energy source and they directly generate an electric signal in response to the measurand[16]. Devices such as the photodiode and thermocouple operate on this principle. In contrast, active sensors require an external excitation signal for their operation; this signal is then modified by the sensor to produce the output signal[16].

A resistive temperature sensor does not generate any electric signal. By passing an electric current through it, its resistance can be measured and the resistance changes can be directly related to temperature based on known functions such as the *Callendar-Van Dusen* equation[16]. Sensors can also be classified as absolute or relative. Absolute sensors detect measurands in reference to an absolute physical scale that is independent of the measurement conditions. While a relative sensor produces a signal that relates to some special case[16]. Sensors can be further classified by whether they are contacting or

non-contacting. The type of sensor used in this work is classified as an active, contacting, absolute, thermo-resistive temperature sensor.

The resistance temperature detector (RTD) is a device in which the electrical resistance is a function of temperature. All metals display a certain amount of resistance to current flow, and this resistance varies directly with the metal's temperature[16]. This phenomenon is the result of the fact that pure metals have a positive temperature coefficient—as the metal's temperature increases, the resistance increases at a fairly linear rate[16,17]. The metals used to fabricate the sensors are chosen for their linear sensitivity, stability, and durability, and they include nickel, platinum and copper[16,17]. Thin film RTD's are often fabricated with nickel or platinum and deposited on a micromachined membrane. They are designed with a serpentine shape for large length to width ratios, which increases the room temperature resistance[17]. The metal chosen for this project was nickel for its high temperature coefficient of resistance, high resistivity, and ease of fabrication.

1.5 Thesis Outline

A micromachined differential scanning calorimeter was designed, fabricated, and applied to monitor the metabolism of biological cells. Chapter 2 discusses the design of the calorimeter. Chapter 3 presents the fabrication of the differential scanning calorimeter. Chapter 4 describes the process of calibrating the sensors and heaters as well as the thermal characterization of the calorimeter. In chapter 5, the initial testing of two separate cells, JM-1 liver cancer cells and normal white blood cells (lymphocytes), is presented. Chapter 6 discusses the methods used to analyze the results to obtain the heat

output and a means to differentiate between the cells. Finally, chapter 7 summarizes the work and offers suggestions for future work.

2 Design of Micromachined DSC

2.1 Principle of Operation

The device fabricated in this work is a micro-calorimeter for bio-sensing applications. The micro-calorimeter is configured as a differential scanning calorimeter. In this configuration the device has twin chambers, one for the sample and one for the reference.

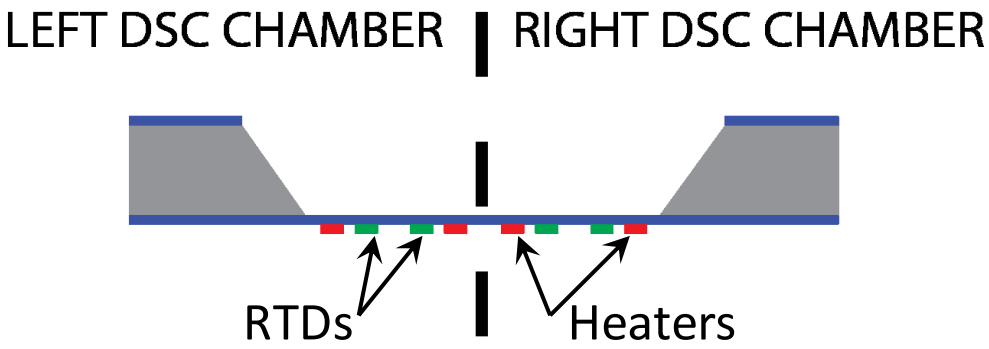

Figure 2.1-1. Schematic layout of DSC device.

The chambers are designed to be matched so that they both have identical physical characteristics, length and width. Both have identical thermal sensor and resistive heater physical characteristics of trace length, width and spacing. The chambers are thermally and electrically isolated from each other and exposed to the same environmental conditions. While the effects of the ambient environment are a major problem of single chamber devices, the advantage of twin chambers becomes apparent

when the difference of the sample signal and the reference signal is obtained—any common environmental effects such as temperature fluctuations are eliminated. This common mode signal elimination is the key to detecting very small thermal changes in the sample.

2.2 Design Considerations

The design of the device is based on the intended application to cell based tests. The device dimensions need to be small to reduce the volume of the samples. Also, the DSC needs to have a small thermal mass and be thermally isolated from the environment to increase sensitivity and thermal time constants. The device must be able to be easily loaded and cleaned while providing an environment for the cells to proliferate. To achieve the small thermal mass and isolation, the sensing areas or chambers were created by etching a cavity through the silicon wafer to expose a silicon nitride membrane.

2.3 Nitride Membrane

The use of a micro-fabricated membrane for the support structure of the calorimeter has many advantages. The membrane is a thin silicon nitride (SiN) film that is created by a low pressure chemical vapor deposition technique (LPCVD) on the surface of the silicon wafer. The backside of this film is then exposed by a wet etching process that removes the silicon in preselected areas to create a suspended membrane structure. The fabrication and deposition processes will be discussed later. This membrane provides a mechanical support structure for the sensors and heaters and provides a platform for samples to be tested. The use of the membrane allows the sensing

area of the device to be thermally isolated from the bulk wafer due to the low thermal conductivity of the nitride film, $30\ W/(m\cdot K)$, as compared to silicon, $149\ W/(m\cdot K)$, since conduction is the primary mechanism of heat transfer during operation. The thermal mass of the device is also reduced through the use of the membrane which is 500nm thick.

2.4 Sensor Design

2.4.1 Thermal Sensing Technologies

Temperature sensing, or thermal sensing, in MEMS devices and micro-fabricated calorimeters is achieved by different technologies, each with their own advantages and disadvantages. These sensing methods fall into one of two classes, thermoelectric sensing and thermoresistive sensing. Thermoelectric sensing is achieved by the use of thermocouples, which make use of the *Seebeck* effect when two dissimilar metal conductors are joined to make a junction. When the sensing junction's temperature changes compared to the reference junction's temperature, a measurable voltage or thermal electromotive force (emf) is generated. This emf is a measure of the increased temperature at the sensing junction. Thermoresistive sensing is achieved by the use of Resistive Temperature Detectors (RTDs), where the conductor's change in resistance is directly related to a change in temperature. Both of these sensing methods use contacting thermal sensors and therefore need to be as close to the measurand as possible.

2.4.2 Operation Theory of RTD

Resistive temperature detectors operate on the principle that a metal's electrical resistance increases with temperature. Resistance is a characteristic which depends on the material and the geometry of the device. The material can be characterized by the resistivity ρ [16]

$$\rho = \frac{m}{ne^2\tau} \qquad (\Omega \cdot m) \qquad (2.1)$$

where m is the mass of the electron, n is the number of conduction electrons per unit volume, e is the electronic charge, and τ is the mean time between collisions (Wilson and Buffa). The conductivity is expressed as the reciprocal of resistivity, $\sigma = 1/\rho$. The resistivity changes with temperature and is expressed by α, which is the temperature coefficient of resistance (TCR)[16,19]:

$$\rho = \rho_0 (1 + \alpha T) \qquad (\Omega \cdot m) \qquad (2.2)$$

where ρ_0 is the resistivity at a reference temperature T_0, which is usually 0ºC. Metals have positive temperature coefficients and a high value α is desired so that a large resistance change is observed for a given change in temperature. The resistance of a conductor can be found by using the following equation[16,19]:

$$R = \rho \frac{l}{a} \qquad (\Omega) \qquad (2.3)$$

where a is the cross sectional area and l is the length of the conductor.

The relationship for the resistance-vs.-temperature characteristics of conductors is given by an approximation of the *Callendar –Van Dusen* equation[16,20]:

$$R_T = R_0(1+\alpha T) \qquad (\Omega) \qquad (2.4)$$

where R_T is the resistance at temperature T $(^{\circ}C)$; R_0 the resistance at $0^{\circ}C$; and α is the TCR. This equation is a linear approximation and is only valid in a narrow temperature range depending on the metal used. For more accurate measurements, a higher order polynomial is required.

Commercial RTDs are platinum wire wound supported by glass with adhesive inside a ceramic tube[16]. They have α values of approximately 0.00392 $\Omega/^{\circ}C$ and remain linear in a temperature range between -100ºC and 600 ºC[17,20]. Thin film RTDs are fabricated of nickel and platinum and deposited on micromachined membranes. The RTDs are fabricated into serpentine shapes to increase the length to width ratios, which increases the base value resistance. Thin film deposited temperature coefficient of resistance values tend to vary depending on the material, deposition process, and purity.

2.4.3 Comparison of RTD vs. Thermocouple

The decision to use an RTD as the primary thermal sensor was based on factors such as the ease of use, the ease of fabrication, and the fact that it is an absolute sensor. Since the RTD operates based on the change in electrical resistance, it only needs to be connected to a sensitive ohmmeter to detect changes. If the ohmmeter is linked to a computer running data acquisition software such as LabView, the temperature values can be directly obtained from the R vs. T calibration equations. For the thermocouple, the emfs that are generated are often very small and therefore require some means of amplification circuitry before the temperature can be extracted. Also, the thermocouple is a relative sensor, which means the temperature obtained from the hot junction is based

on, or relative to, the temperature at the cold junction. Therefore, the temperature of the cold junction must always be known. The fabrication of the RTD is much easier than that of a thermocouple. Since a thermocouple is made of two dissimilar metals, it requires two photolithographic steps and two deposition processes. Multiple processing steps increase the potential for errors and reduced yield because the two individual lithography masking steps need to be aligned correctly to create the hot and cold junctions. In addition, if a heater is to be incorporated, it potentially adds an additional lithographic and deposition step to the overall fabrication of the device.

Because the RTD is thermoresistive sensor, only one metal is required to fabricate it, which reduces the process to one lithographic and deposition step. Also, the integrated heater can be made from the same metal as the RTD and fabricated in the same lithographic process. Several metals are typically used for thin film RTD's including nickel, copper, and platinum. For this work nickel was chosen for its high temperature coefficient of resistance, relatively high resistivity, and ease of deposition. A comparison of the material properties for typical thin film RTDs are given below.

Metal	Temperature Coefficient of Resistance at 20ºC (Ω/ºC)	Resistivity at 20ºC (Ω-cm)	Thermal Conductivity (W/m-K)	Specific Heat Capacity (J/g-K)
Nickel	0.00690	6.40 x 10-6	60.7	0.460
Platinum	0.00392	10.6 x 10-6	69.1	0.134
Copper	0.00393	1.70 x 10-6	388	0.385
Gold	0.00340	1.72 x 10-6	301	0.132
Cupronickel	*	37.5 x 10-6	*	*
Nichrome	0.0004	100 x 10-6	*	*

Table 2.4-1. Material properties for selected metals[21,22].

2.5 Heater Design

2.5.1 Resistive Heating for Integrated Heater

When electric current is sustained in a conductor, the electrons are given energy by the power supply or voltage source. As these charge carriers pass through the conductor, they collide with the atoms of the material, i.e., they encounter resistance, and lose energy (Wilson and Buffa). The energy transferred in the collisions results in an increase in the temperature of the conductor. In this fashion the electrical energy is converted into thermal energy[19].

The energy gained by an amount of charge, q, from a voltage source, V, is qV. The average rate of energy delivered to a resistive conducting element is called the *average power*, $\bar{P}$ and is given by[19]:

$$\bar{P} = \frac{qV}{t} \qquad (J/s) \qquad (2.5)$$

When the current and voltage are steady with time, then the average power is constant. For DC currents, $I = q/t$, the previous equation becomes[19]:

$$P = IV \qquad (J/s) \qquad (2.6)$$

Using Ohms law, $R = V/I$, we can rewrite the equation for power dissipation:

$$P = IV = \frac{V^2}{R} = I^2R \qquad (J/s) \qquad (2.7)$$

This thermal energy dissipated by a current carrying resistor or conductor is referred to as Joule heating. Since the resistance can be measured and the voltage applied

is also known, we can easily produce a specific value of heat. By incorporating the heater on the membrane of the device and using the effects of Joule heating, we can use the heater to provide a known heat to the samples and for calibration purposes.

2.5.2 Geometry

The geometry of the integrated heater element is designed so that it will produce a uniform temperature distribution in the sample and reference chambers. The shape of the heater often takes a similar shape to the sensor. In this work, several designs were explored. Meandering serpentine traces were first designed with a small number of passes. It was found that heating was not very uniform, therefore the trace pass numbers were increased as well as the length. This greatly increased the uniformity of the temperature field. Circular patterns were also fabricated and found to have a uniform field.

2.6 Numerical Analysis (ANSYS)

Heater designs were numerically analyzed using a finite element modeling software package, Ansys, to verify the temperature distribution. The first design for the sensor and heater was made small so that it was on the order of the cellular sample to be measured. Dimensions of the traces were 5μm wide with 5μm spacing, and the overall dimension of the active sensor area was approximately 55μm x 45μm. The RTD and heater were simulated using nickel as the thin film metal on a rectangular membrane of silicon nitride to simulate the chamber area. Material properties for nickel and silicon nitride used in the simulation are given in the following table.

Material	Thermal Conductivity (W/m-K)	Resistivity at 20ºC (Ω-cm)	Specific Heat Capacity (J/g-K)	Density (g/cm^3)
Nickel	60.7	6.40×10^{-6}	0.460	8.88
Silicon Nitride	16	10×10^{12}	0.7	3.2

Table 2.6-1. Material properties for materials used during numerical analysis[21,22].

As figure 2.6-1 shows, the temperature distribution are centered more around the heater, which is to be expected. While it appears to have a good distribution, the area of the RTD where the samples are to be positioned spans three different temperature values. From the center moving outward, each color represents approximately a three degree drop in temperature. At a distance of approximately 30μm from the center, the temperature has dropped by nearly 10ºC. This can be a major problem for cell based tests because certain cell types require a stable temperature and are very sensitive to fluctuations.

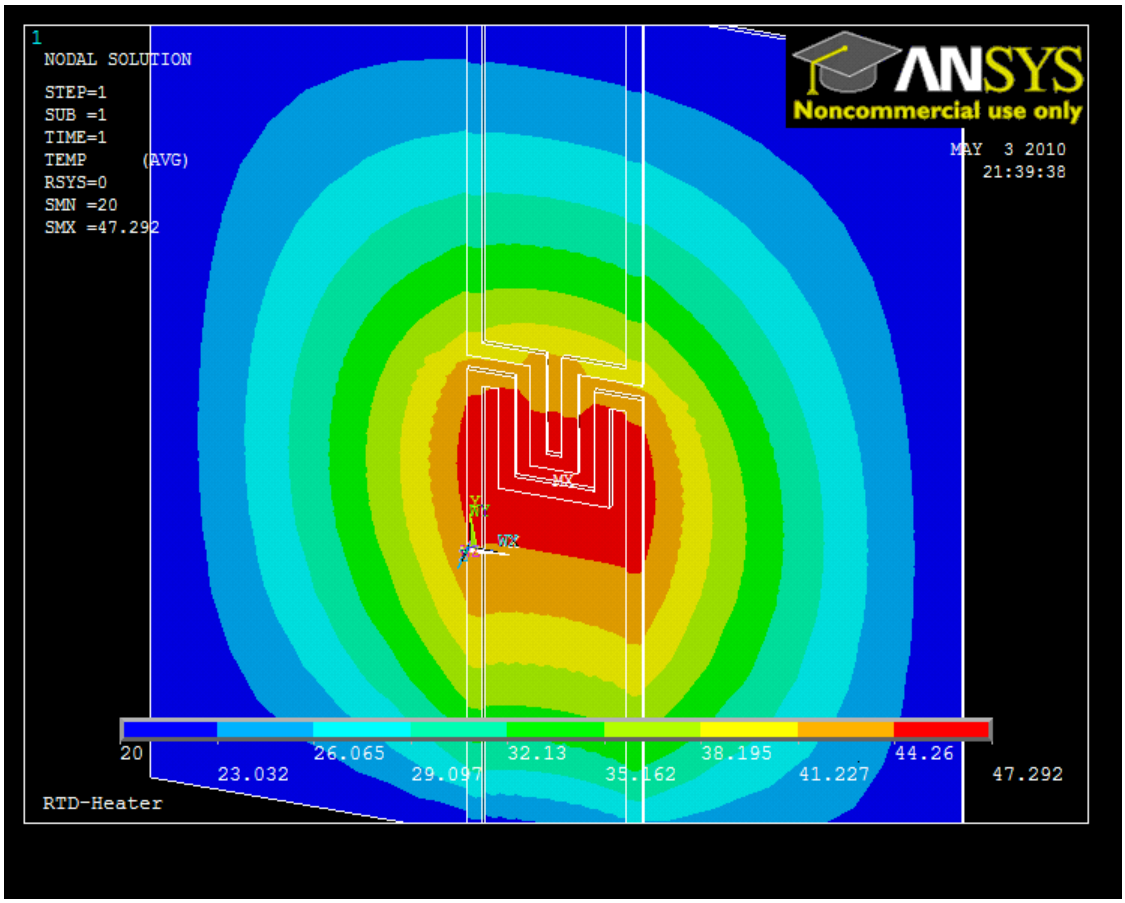

Figure 2.6-1. Ansys results from simulation of heater. RTD is top trace, heater is bottom trace. Voltage applied to heater was 4V, temperature is in degrees Celsius.

In the next simulation the trace lengths were increased by adding an additional serpentine pass to the heater and RTD. Figure 2.6-2 shows the results from the simulation. While the temperature distribution is similar to the previous results, the change in temperature as moving out from the center is reduced to two degrees per unit.

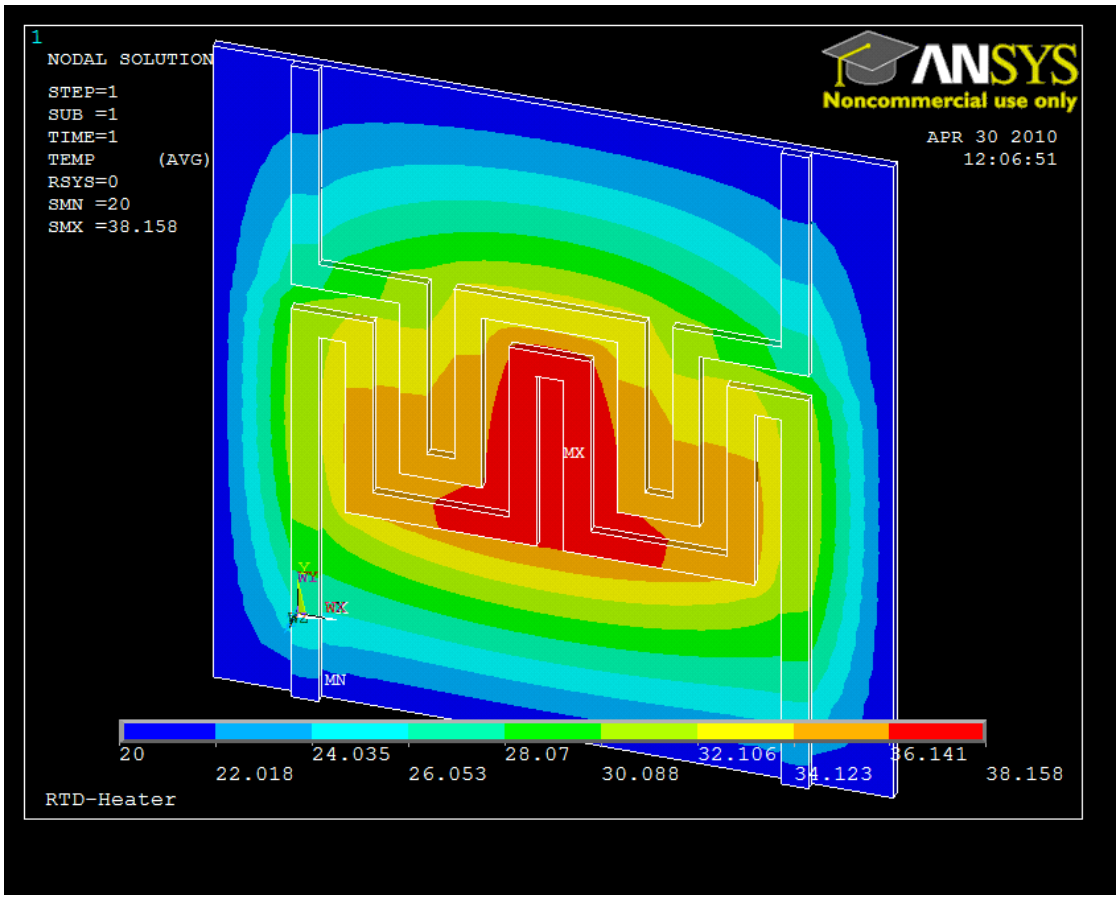

Figure 2.6-2. Ansys results from simulation of heater. Trace lengths were increased by adding an additional pass. Heater is bottom trace, RTD is top trace. Voltage applied to heater was 5V, temperature is in degrees Celsius.

While it is an improvement, the temperature field is still irregular and not uniform. In an attempt to improve on the temperature uniformity, a second heating element was added to the design. When this geometry was simulated it showed dramatic improvement on the uniformity of the temperature field, figure 2.6-3. However, the distribution of the temperatures was still poor, showing a change of more than a degree per unit.

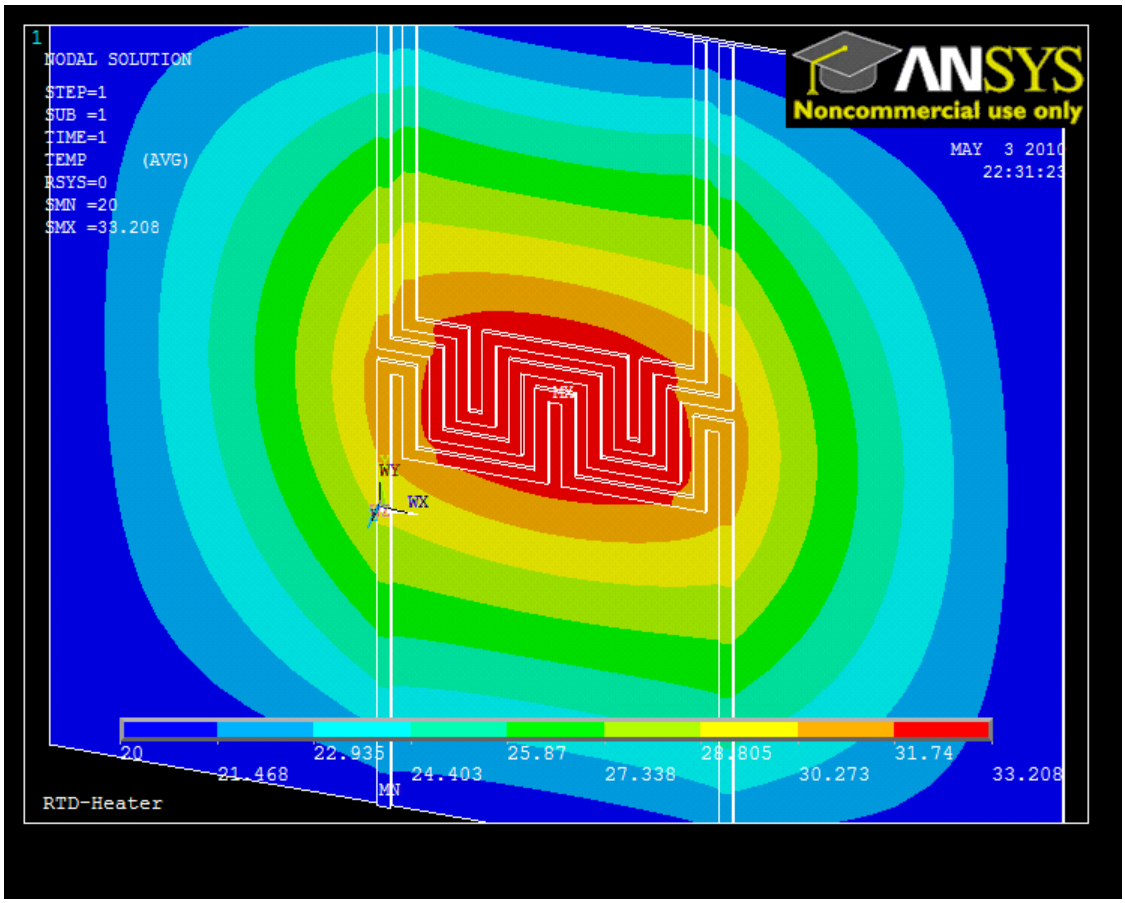

Figure 2.6-3. Ansys results from simulation of heater. Trace lengths were increased by adding additional pass, also second heater was added. Heater is bottom and top trace, RTD is middle trace. Voltage applied to heater was 5V, temperature is in degrees Celsius.

Next, the number of serpentine passes were increased, as well as the length of the elements. Figure 2.6-4 shows the results from this simulation. The temperature field is uniform and the distribution is reduced to 0.7ºC per unit. This is a great improvement over the original design, as the temperature only drops by five degrees when removed from the center of the geometry by more than 100µm compared to 10ºC over 30µm.

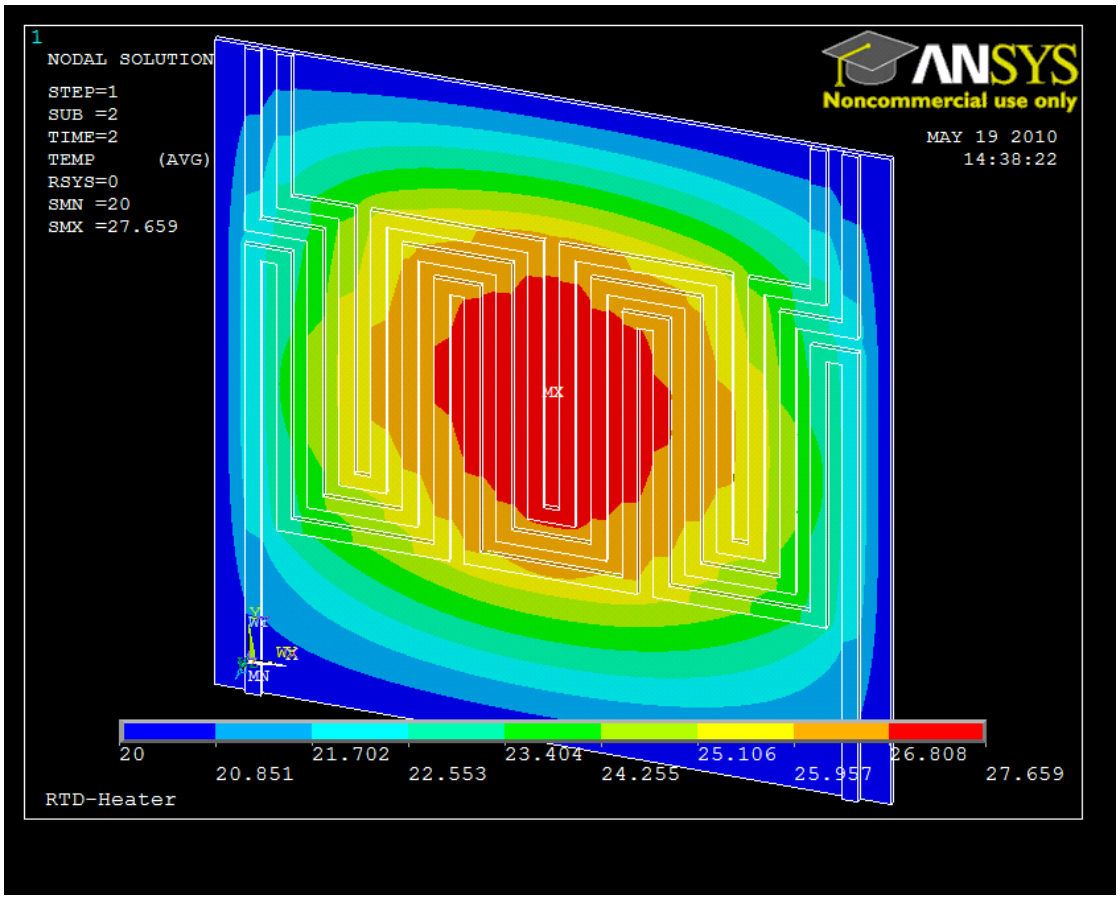

Figure 2.6-4. Ansys Results from simulation of heater. Trace lengths were increased by adding additional passes, also second heater was added. Heater is bottom and top trace, RTD is middle trace. Voltage applied to heater was 5V, temperature is in degrees Celsius.

The use of Ansys to simulate and predict the behavior of the heater was a major advantage. It allowed us to change designs based on the results of simulations, and we could rapidly achieve a final design without the need for successive fabrication and testing of physical devices. In the end, the final chosen design was similar to figure 2.6-4, but the second heater was omitted.

3 DSC Device Fabrication

In this section a brief overview of the techniques used to fabricate the device including equipment and processes is discussed. Later, a process flow is shown including steps required for fabrication as well as specific process details.

3.1 Use of Silicon

Silicon is the most widely known semiconducting material in use today. It is the most abundant element on Earth, and it can be refined from sand to produce electronic grade single crystal wafers. Single crystal silicon is perhaps the most versatile material for bulk micromachining, due to its well-characterized anisotropic etches and etch masking materials[23]. Two key capabilities make bulk micromachining a viable technology: (1) the availability of anisotropic etchants such as potassium hydroxide (KOH), which preferentially etch single crystal silicon along select crystal planes; and (2) the availability of silicon etch mask and etch stop materials that can be used in conjunction with the etch chemistries to protect select regions of the substrate from removal[18].

Other advantages for the use of silicon as a fabrication substrate for sensor applications include its mechanical stability and the ability to integrate processing electronics on the same wafer. It has approximately the same Young's modulus as steel, with a thermal expansion coefficient 8 times smaller and virtually no mechanically hysteresis[18]. Silicon is extremely flat and can readily accept various coatings and thin

films for building microstructures or conducting electricity[18]. Therefore, it is an ideal material for sensors and actuators.

3.2 Bulk Microfabrication Methods

3.2.1 Deposition/Oxidation

Deposition and oxidation are two popular methods used to create thin films for membranes, electrical insulation, or etch masks. Oxidation, or more specifically thermal oxidation of silicon, is used to create silicon dioxide thin films. Silicon dioxide growth involves heating the wafer to 900ºC in an electric resistance furnace while passing a stream of steam at atmospheric pressure[18,23]. The high temperature aids the diffusion of oxidant to the surface of the silicon wafer where the following chemical reaction takes place[18,23]:

$$Si_{(solid)} + 2H_2O_{(steam)} \rightarrow SiO_2 + 2H_{2(gas)}$$

This process consumes a portion of the silicon substrate to create the film. The time, temperature, and gas flow rate are controlled to create the desired quality and thickness of film. The resulting SiO_2 film has high compressive stress due to molecular mismatch and thermal expansion differences.

Chemical vapor deposition (CVD) is another process that is used to create thin films; however, in this process the film is added to instead of consuming the substrate. CVD involves the flow of an inert carrier gas with diffused reactants over a hot substrate surface to deposit a solid film[18,23]. The energy supplied by the surface temperature

promotes chemical reactions through diffusive-convective transport to form films during and after the reactions[18,23]. Silicon nitride (Si_3N_4) is formed by using a reactant of silane (SiH_4) and a carrier gas of ammonia (NH_3) with a furnace temperature of 700-900ºC under the following reaction[18]:

$$3SiH_4 + 4NH_3 \rightarrow Si_3N_4 + 12H_2$$

The CVD process works at low or atmospheric pressure and a relatively low temperature. This has the advantage of higher growth rates with better quality films and tensile stresses.

3.2.2 Photolithography

The photolithographic process is the most important step in creating micro-fabricated devices on substrates with sub-micrometer resolutions. This process involves the transfer of an optical image from mask to a light sensitive film called photoresist on the surface of a wafer to produce a pattern. The wafer and the photoresist are then exposed to ultra violet light through a transparent mask causing the opaque images to be transferred in a machine called a contact aligner. If the solubility of the photoresist is increased under the exposure to UV light it is called a positive photoresist, while negative photoresist becomes more soluble under the shadow of the mask. The exposed wafer is then developed with chemical solvents to reveal the transferred image. A permanent image is then created by further etching of the wafer. Depending on the photoresist used, different images can be achieved when using the same mask image.

This process is called optical contact lithography; other technologies for lithography are also available such as electron beam, and ion beam lithography. These processes transfer features by direct writing of the image without a mask and have typical linewidths of 0.1μm compared to 2-3μm of optical lithography[23]. While they may produce higher resolution features the equipment is more complex, requires the process to operate in a vacuum environment and is generally slower due to the direct writing. Due to the size of the features for this DSC device, >10μm, optical contact lithography is the chosen technique because it is readily available, the cost of masks and chemicals is lower, and multiple wafers can be rapidly processed.

3.2.3 Etching

One of the most important characteristics of etching is the directionality (or profile) of the etching process. If the etch rate in all directions is equal, the process is said to be isotropic. Etch processes that are anisotropic generally have etch rates perpendicular to the wafer surface that are much larger than the lateral etch rates.

Anisotropic silicon etchants attack the (100) and (110) crystal planes significantly faster than the (111) crystal planes. For example the (100) plane to (111) plane etch ratio is about 400:1 for a typical KOH/water etch solution[23]. Silicon dioxide, silicon nitride, and some metallic films (Cr, Au) provide a good etch mask for most silicon anisotropic etchants[18]. For long etching time in KOH, SiN is the preferred mask due to its chemical durability[23].

A large number of dry etch processes are available to pattern single crystal silicon. The process spectrum ranges from physical etching via sputtering and ion beam

milling to chemical plasma etching. Two processes, reactive ion etching and reactive ion beam etching, combine aspects of both physical and chemical etching. In general, dry etch processes utilize a plasma of ionized gases along with neutral particles to remove material from the etch surface[18].

Reactive ion etching is the most commonly used dry etch process to pattern silicon[23]. In general, fluorinated compounds such as CF_4, SF_6 and NF_3 or chlorinated compounds such as CCl_4 or Cl_2 sometimes mixed with He, O_2, or H_2 are used[23].

3.2.4 Metallization

The creation of the nickel RTDs and heaters is done through a combination of metallization of the entire wafer and a selective removal of the deposited metal. The metallization of the wafer is done in a thermal evaporator. The wafers are loaded into a high vacuum chamber that is pumped down by a diffusion pump to 10^{-7} Torr. The material to be evaporated is loaded into a crucible that is heated by an embedded resistance heater. When the material becomes hot it gives off a vapor. Since the internal pressure is so low, the mean free path between molecular collisions is much greater than the distance to the wafer therefore the vapor travels in a straight path until it strikes the wafers and slowly forms a film. Processes like sputtering use higher pressures and therefore have shorter mean free paths[23]. Therefore sputtering can create films with step coverage[23].

Instead of evaporating the film directly on the wafer, and then etching a pattern after lithography, the film is directly evaporated on the patterned, developed photoresist. The films tend to break at the edges of the photoresist, so that when the wafer is placed in

a solvent, the photoresist is dissolved and unwanted film is easily removed. This process is called lift-off and is a very effective method to produce metal features when etch chemicals are not available or when over etching could be problematic.

3.3 Process Flow Diagram

What follows is a detailed outline of the fabrication process used to create the DSC device. It utilizes conventional semiconductor fabrication equipment, chemicals and processing techniques. The fabrication requires two mask steps, two etching steps, one metallization, and a lift off.

A) A [100] oriented p-type silicon wafer is coated with a low stress silicon nitride film approximately 500nm thick. It is cleaned using a bath containing sulfuric acid and hydrogen peroxide to remove any organic contaminants that may be present. The wafer is spin coated on bottom side with AZ 2514 IR photoresist for 30 seconds. The wafer is soft baked at 110ºC for 1 minute to remove any solvent. A photo-lithographic mask is aligned with the <110> and placed in direct contact with the resist coated surface. It is exposed to ultra violet radiation for 10 seconds using a Cobilt mask aligner. It is developed using AZ 400K developer for approximately one and a half minutes. The front side is also coated with photoresist to protect it from damage during the dry etching process.

B) After a hard bake for 2 minutes at 110ºC, the wafer is placed in a reactive ion etcher (RIE), and etched in carbon tetraflouride with a system power of 300W at 0.06 Torr. It is etched for 12 minutes, then rotated 180º and etched for an additional 12 minutes to remove the SiN and open a window to reveal the silicon beneath.

C) With the silicon now exposed underneath the silicon nitride, the next process it to remove the photoresist that was used as a mask from the previous step. The wafer is placed in a bath of 80ºC piranha for approximately 20 minutes. After rinsing with DI water, the wafer is placed in 30% potassium hydroxide (KOH) at 60ºC for 24 hours.

D) Now that the supporting membrane has been fabricated, the RTD and heater need to be printed. The wafer's front side is spin coated with AZ 2514 IR photoresist with the same parameters as defined for the backside process. To define the traces, a positive mask is used to transfer the pattern to the surface of the wafer. However, a negative image is required to ensure effective lift off of the nickel deposition. To achieve an image reversal, the wafer is exposed to ultra violet radiation for 10 seconds through the positive mask. The wafer is soft baked for 2 minutes at 130ºC, and then is subjected to UV radiation without the mask for 36 seconds. It is developed for 30 seconds to complete the image reversal process.

E) A Nickel layer is then deposited over the entire surface through thermal evaporation. The lift off of excess material is achieved by soaking the wafer in 1165 solvent for approximately 4 hours. The solvent breaks down the underlying layer of photoresist and since the Ni is bonded to both the surface of the wafer and the PR, the Ni bonded to the Pr is washed away to reveal the trace networks of the RTDs, heaters and contact pads of Ni that are still bonded to the silicon.

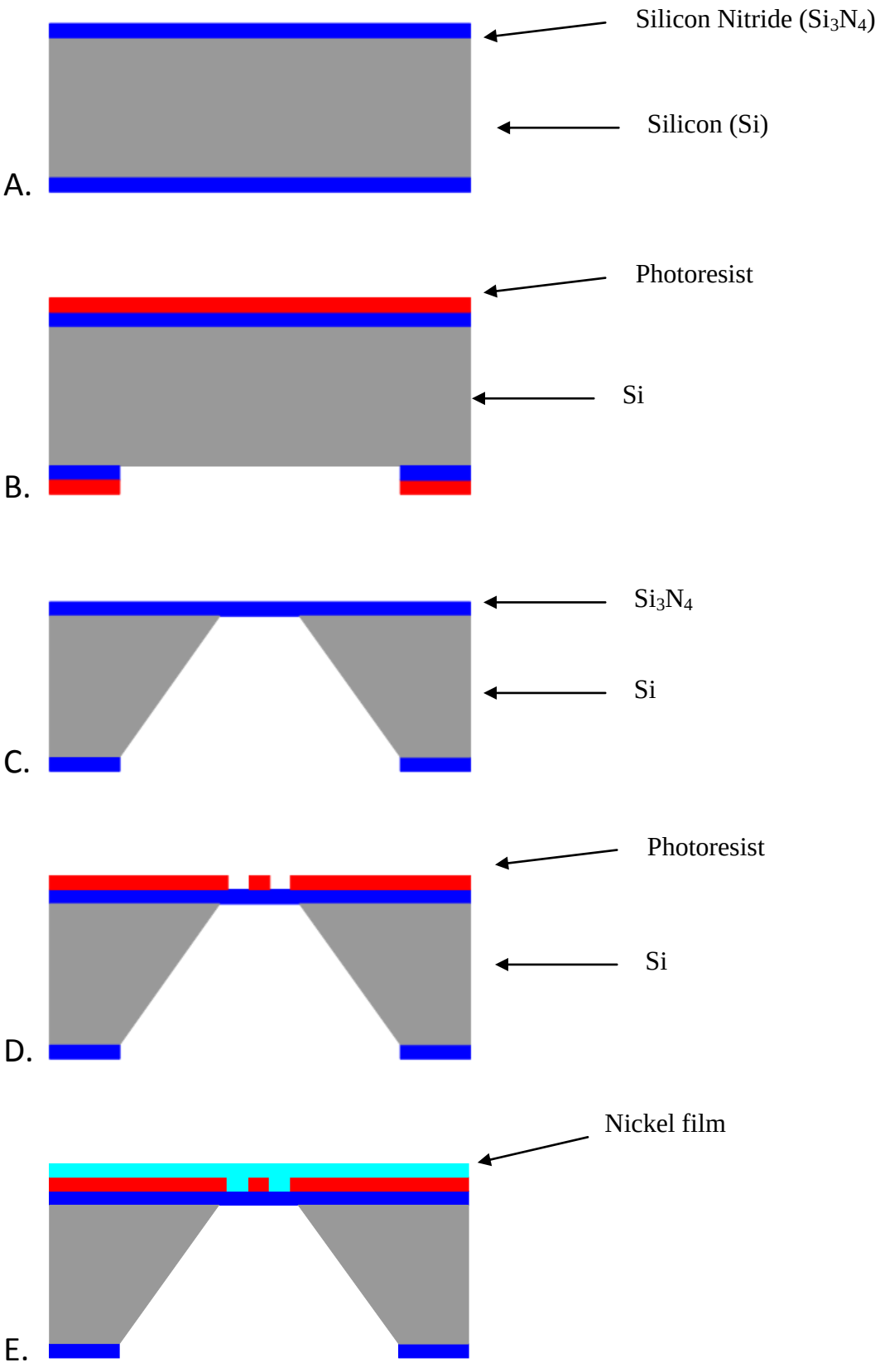
Silicon Nitride (Si_3N_4)
Silicon (Si)
A.
Photoresist
Si
B.
Si_3N_4
Si
C.
Photoresist
Si
D.
Nickel film
E.

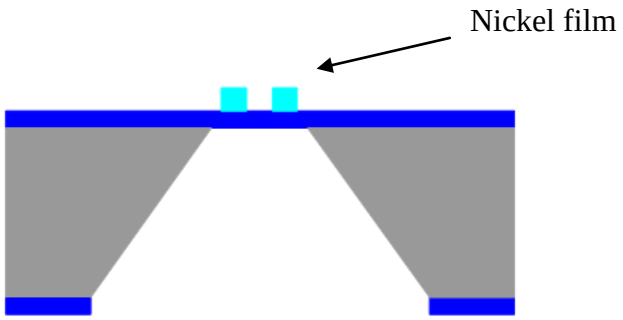

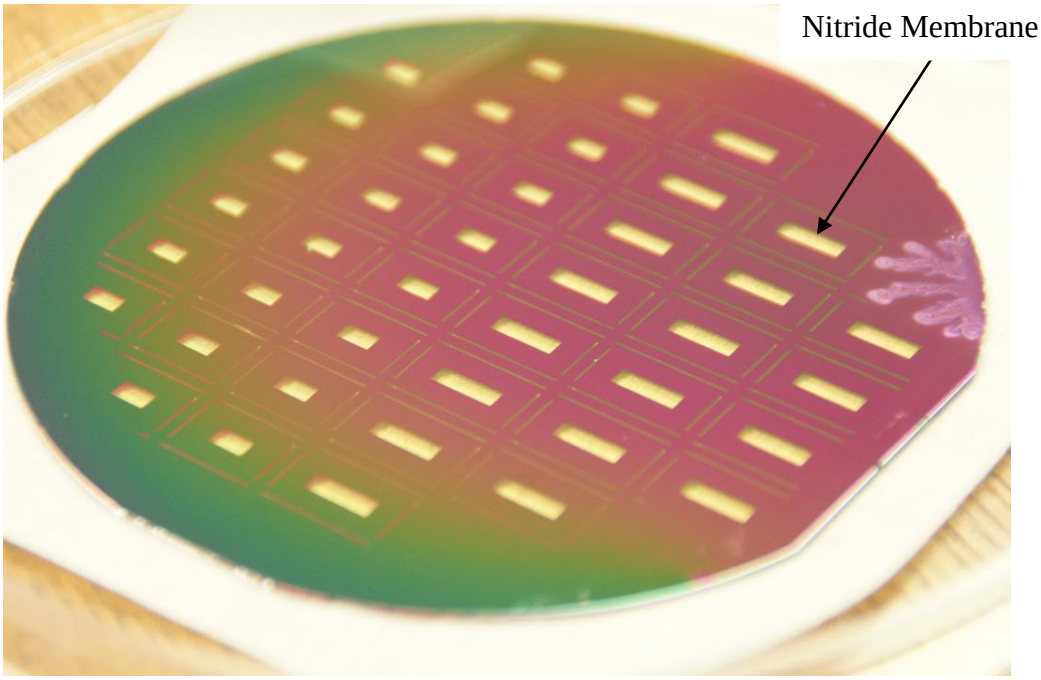

Figure 3.3-1. Topside view of wafer after backside etch.

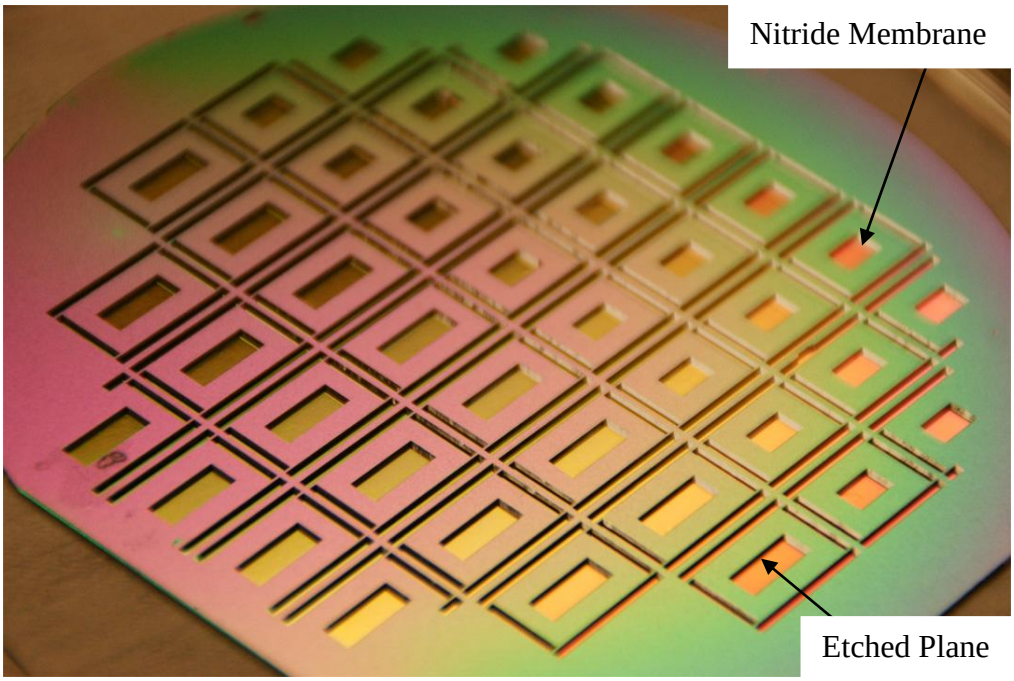

Figure 3.3-2. Backside view of wafer after backside etch.

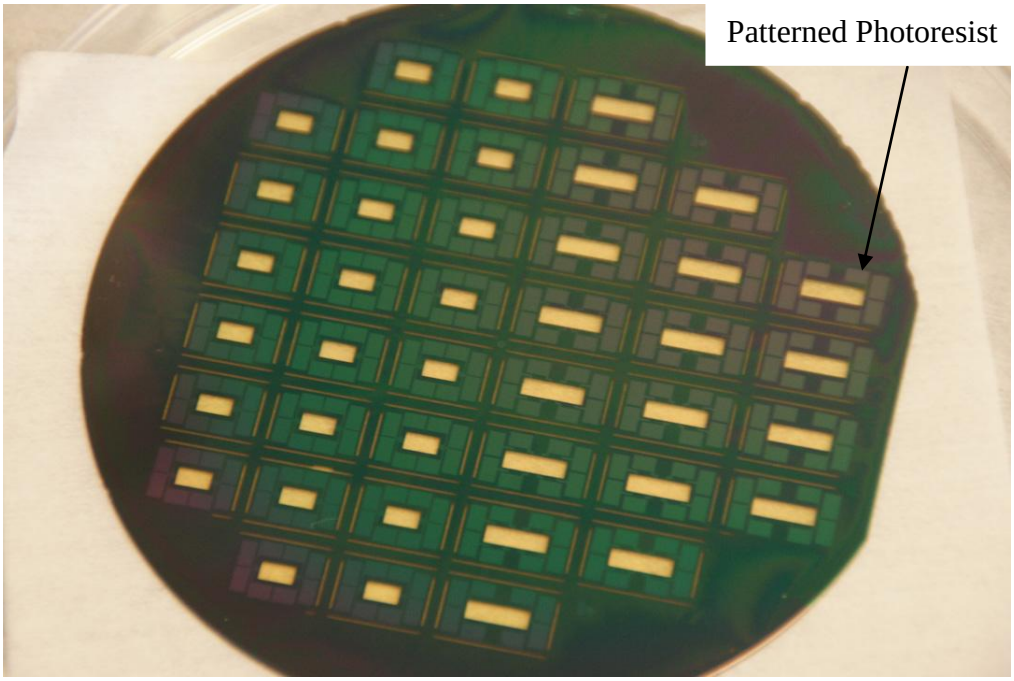

Figure 3.3-3. Topside of wafer after image reversal photolithographic process.

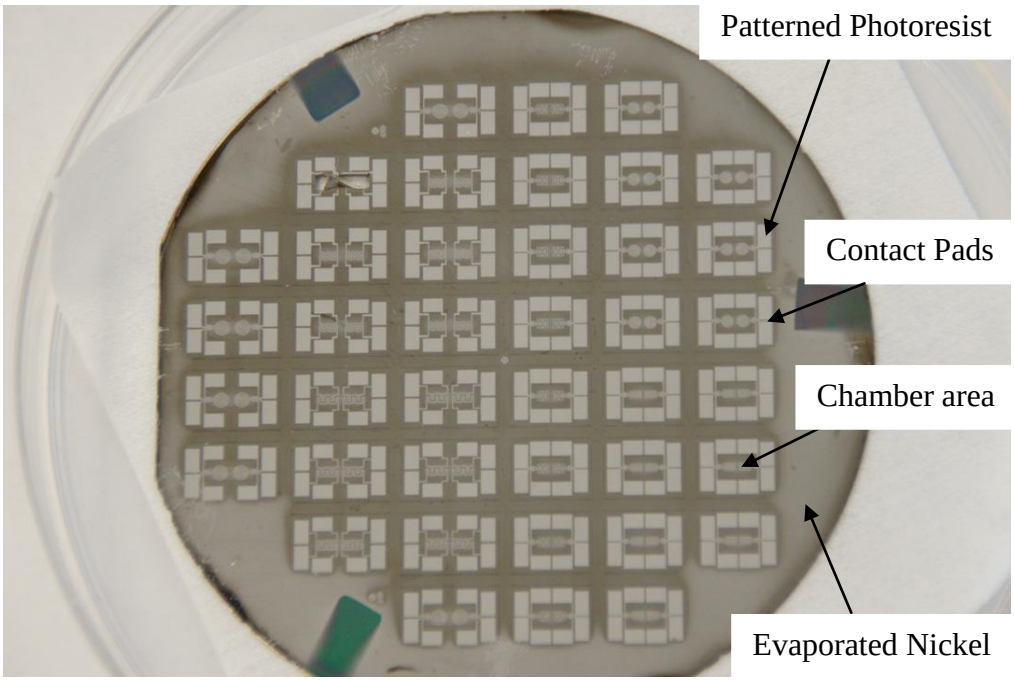

Figure 3.3-4. Topside of wafter after nickel evaporation.

4 DSC Characterization

This chapter discusses the characterization of the DSC device. The calibration procedure for the sensors and heaters are presented with results for the devices used in future experiments. A step response of the DSC was also performed to extract its thermal properties.

4.1 Electrical Resistance of Conductors

Conductors are materials with large values of conductivity. The magnitude is usually on the order of $(10x10^6)/\Omega*m$ for typical conductors. The specific expression of conductivity for conductors is:

$$\sigma = n_e q_e \mu_e \quad (\Omega \cdot m)^{-1} \tag{4.1}$$

where the density of charge carriers is n_e, while q_e is the charge carried by each, and μ_e is the mobility of each carrier[16,21]. The subscript *e* refers to purely electronic conduction, which is conduction specifically resulting from the movement of electrons. A temperature rise above room temperature on metals results in a drop in conductivity[22]. This drop in conductivity is the result of a drop in electron mobility, μ_e, with increasing temperature[22]. The drop in electron mobility can be attributed to the increased thermal agitation of the crystalline structure of the metal as the temperature increases[22].

Resistivity and conductivity are inversely related through the equation:

$$\sigma = \frac{1}{\rho} \quad (\Omega \cdot m)^{-1} \tag{4.2}$$

where ρ is the resistivity and its magnitude is on the order of $0.1x10^{-6}\Omega$-m for typical conductors[16]. The resistivity increases as temperature increases above room temperature. The relationship $[\rho(T)]$ is used more frequently than $[\sigma(T)]$ because resistivity is found experimentally to increase quite linearly with temperature[16].

$$\rho = \rho_{rt}[1+\alpha(T-T_{rt})] \quad (\Omega \cdot m) \qquad (4.3)$$

where ρ_{rt} is the room temperature value of resistivity, α is the temperature coefficient of resistivity, T is the temperature, and T_{rt} is the room temperature[16]. This relationship can be extended to an approximate resistance vs. temperature characteristic for conductors between 0ºC and 100ºC.

$$R_T = R_0(1+\alpha T) \quad (\Omega) \qquad (4.4)$$

These relationships and equations form the basis for resistive temperature detector.

4.2 RTD Calibration

It is understood that the relationship between resistance and temperature for a metal conductor is positive and linear within a specific temperature range. However, the devices exact change in resistance for a given change in temperature is unknown. Therefore the devices need to be calibrated so we can accurately predict the response of the RTD. To calibrate the RTDs the device is heated to known temperatures while observing the value of resistance. That procedure is described in this section.

The process begins by dicing the wafer to remove the individual devices from the bulk of the substrate. The chips are then bonded with silver epoxy to a printed circuit board (PCB), as shown in figure 4.2-1. This helps to make good electrical contact from

the RTDs and heaters to the test equipment through two rows of four pin headers. The PCB also has the advantage of improving the handling of the device for calibration and testing purposes.

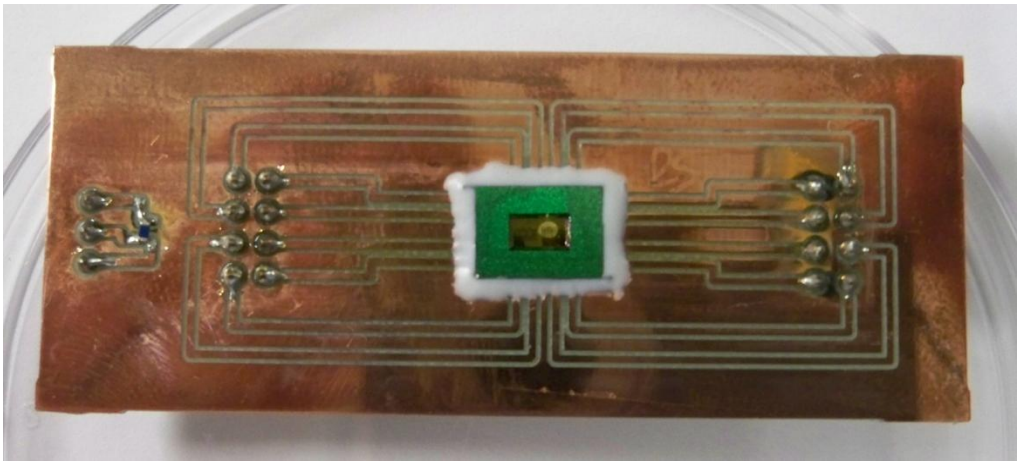

Figure 4.2-1. Chip bonded to PCB.

The RTD to be calibrated is connected to a Keithley 2400 SourceMeter and the on board surface mount Pt 100 RTD is connected to an Omega CN2011temperature recorder, as shown in figure 4.2-2.

The surface-mounted RTD will give an accurate temperature value inside the vessel during the calibration procedure. The PCB is then loaded into a thick stainless steel vessel and is sealed shut, as shown in figure 4.2-3. This vessel has a high thermal mass and once it reaches a steady state temperature, any small temperature variations are dissipated and the internal temperature will remain constant.

The heating of the vessel and contents is done by placing the entire unit into a HAAKE C50 regulated water bath, shown in figure 4.2-4. The temperature of the bath is controlled using a LabView program and is ramped from 10ºC to 50ºC. The temperature

of the vessel is allowed to reach equilibrium at 10ºC before initiating the scan. There is a lag between the actual water temperature and the actual internal vessel temperature due to the thermal mass of the vessel. A commercially available surface mount RTD is used to monitor the internal temperature. The value of resistance for the RTD and the internal temperature are both recorded with a LabView program.

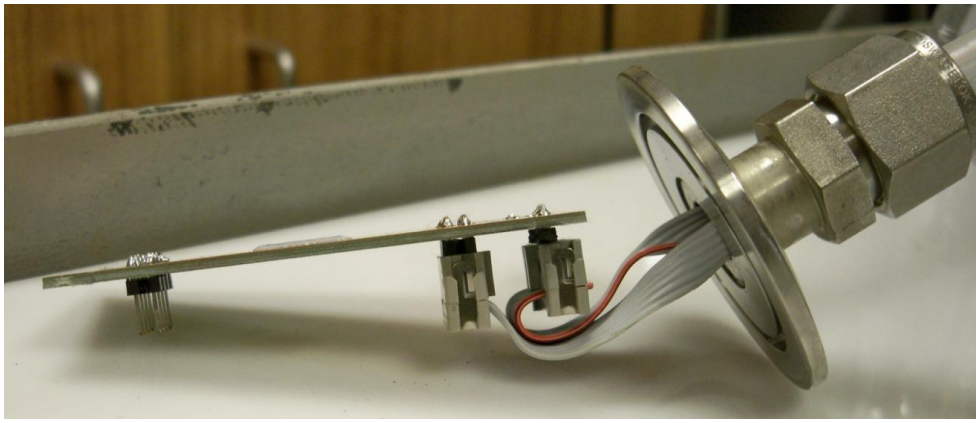

Figure 4.2-2. Connecting the device to the test equipment for calibration.

Figure 4.2-3. PCB and chip loaded into stainless steel vessel for calibration.

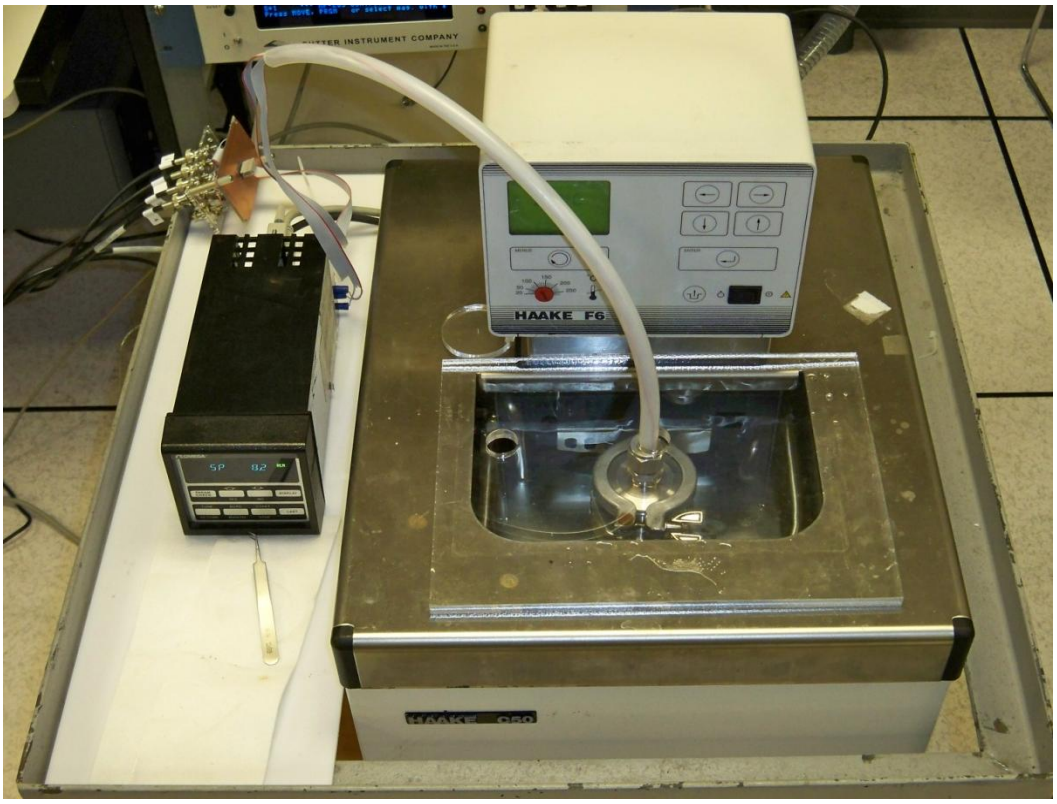

Figure 4.2-4. Entire calibration setup showing water bath, carrier vessel and temperature recorder.

Once the calibration scan is completed, the data can be plotted and curves fitted to extract specific properties of the DSC RTD. These properties include the temperature coefficient of resistance (TCR), also known as its alpha value, zero degree Celsius resistance value (R_0), and its apparent linearity. For example, the calibration of one particular device gave the results shown in figure 4.2-6 and 4.2-7. This device uses a circular trace pattern for the RTD and heater elements, as shown in figure 4.2-5. The pattern diameter is approximately 1200µm.

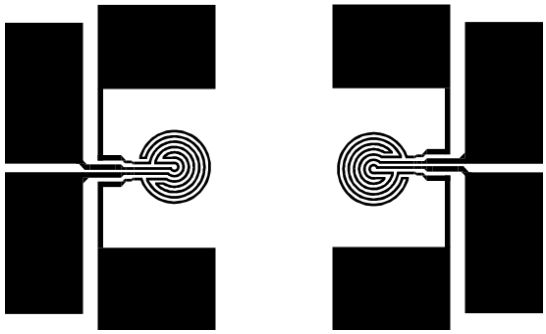

Figure 4.2-5. Device SCA schematic layout, showing left and right chambers.

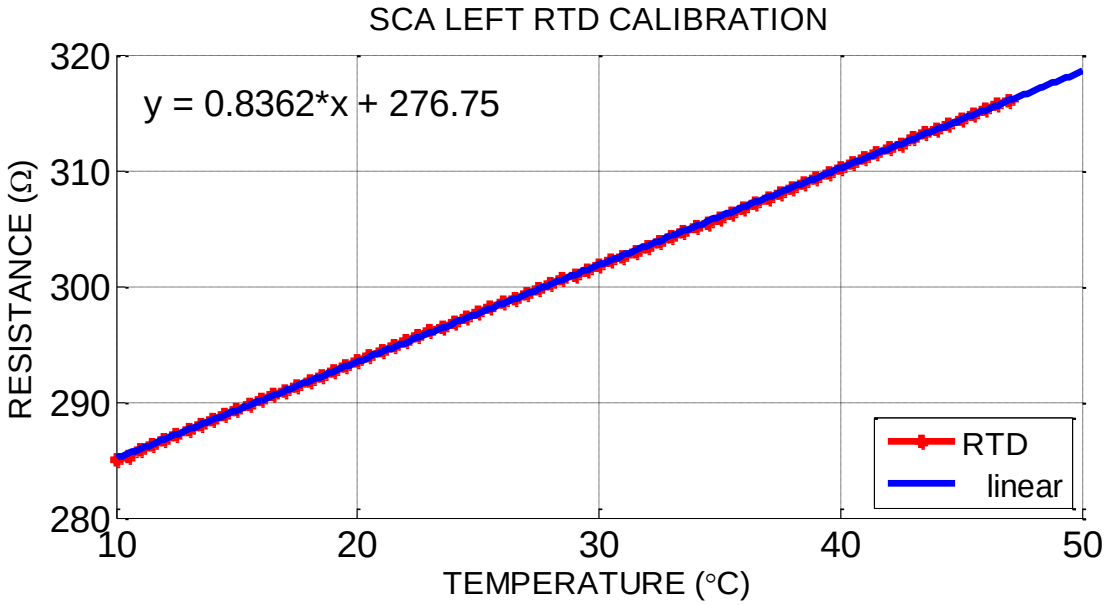

Figure 4.2-6. Left chamber RTD calibration results.

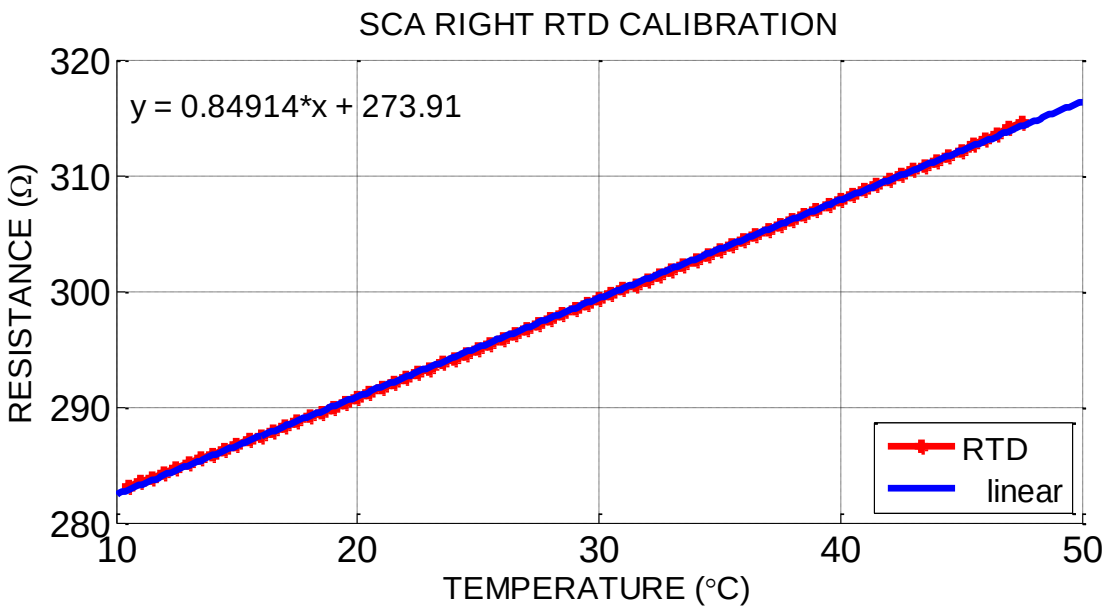

Figure 4.2-7. Right chamber RTD calibration results.

When the results from the calibration runs are examined, it becomes apparent that both devices are extremely linear. The required parameters can be extracted when a linear curve is fit to the data. In this case, both devices showed similar parameters which was to be expected due to the nature of microfabrication.

Device	α (ºC)$^{-1}$	R_0 (Ω)	Thickness	Film material
SCA Left Chamber	3.0215 x 10^{-3}	276.75	70nm	Thermally Evaporated Nickel
SCA Right Chamber	3.1000 x 10^{-3}	273.91	70nm	Thermally Evaporated Nickel
SS2-C Left Chamber	1.5161 x 10^{-3}	362.84	50nm	Thermally Evaporated Nickel
SS2-C Right Chamber	1.5058 x 10^{-3}	365.33	50nm	Thermally Evaporated Nickel

Table 4.2-1. RTD parameter results from calibration for selected DSC devices.

Each device used for testing was individually calibrated before testing. Several other design geometries and film thicknesses were also explored. They were also

calibrated using this process and their results will be presented later in terms of optimal design.

4.3 Heater Calibration

The integrated resistive heaters provide the ability to scan the temperature of the samples at a predetermined rate or maintain a certain temperature. For example, during cell-based tests the temperature should be maintained about 37ºC, the temperature of the human body. The heaters need to be calibrated to ensure that we are providing an accurate temperature to the chamber areas. This process will be discussed in detail next.

A voltage is applied to the resistive heaters, which increases the temperature of the chamber through dissipative heating effects. When a current is passed through a resistive element, the opposition to current flow of the metal produces heat. This is known as Joule heating, and the amount of heat released is proportional to the square of current times the resistance. By using Ohms law we can solve the relationship in terms of voltage.

$$Q \propto I^2 \cdot R \rightarrow Q \propto \frac{V^2}{R} \qquad (J) \qquad (4.5)$$

By applying different values of voltage to the integrated heaters and observing the calibrated RTDs, we can extract the temperature values and calibrate the heaters.

Figure 4.3-1 schematically shows the testing setup to calibrate the heaters. An Agilent power supply is connected to the integrated heater and an Agilent multimeter is connected to the RTD. A computer running LabView is used to control and record data from both pieces of equipment.

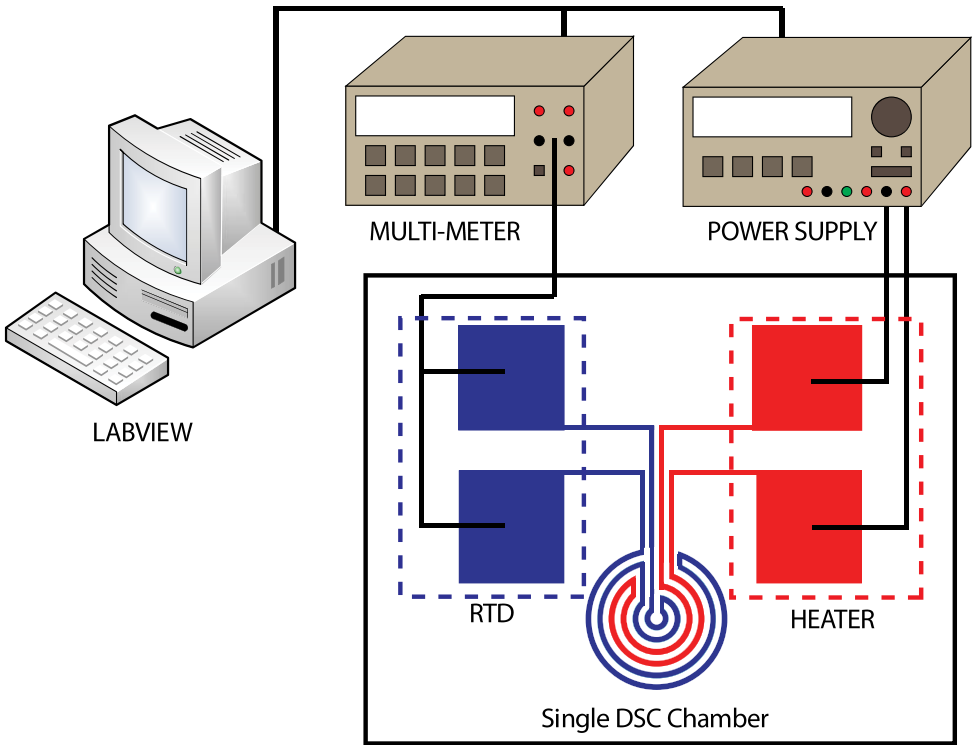

Figure 4.3-1. Schematic layout for heater calibration.

A DC voltage from zero to ten volts is applied in 0.5 volt increments for ten seconds per increment. The response of the RTDs to the applied voltage is plotted in figures 4.3-2 and 4.3-3 for the left and right chambers respectively. Having previously calibrated the RTDs, we can now extract the temperature of the integrated heater at each voltage level. The results are plotted in figures 4.3-4 and 4.3-5 for the left and right chambers respectively. They show an exponential increase in temperature for a linear increase in voltage, which is due to the squared relationship of voltage to power as expressed earlier in the equation for Joule heating. By fitting a quadratic curve to the data, we obtain an equation that will allow the prediction of temperature given the applied voltage or the required voltage for a desired temperature. The following table shows an example of the voltage required to heat the chamber the approximately the temperature of the human body.

Device	Chamber Temperature (ºC)	Required Heater Voltage (V)
SCA Left Chamber	37ºC	1.91
SCA Right Chamber	37ºC	1.81
SS2-C Left Chamber	37ºC	1.46
SS2-C Right Chamber	37ºC	1.53

Table 4.3-1. Required voltage for desired chamber temperature.

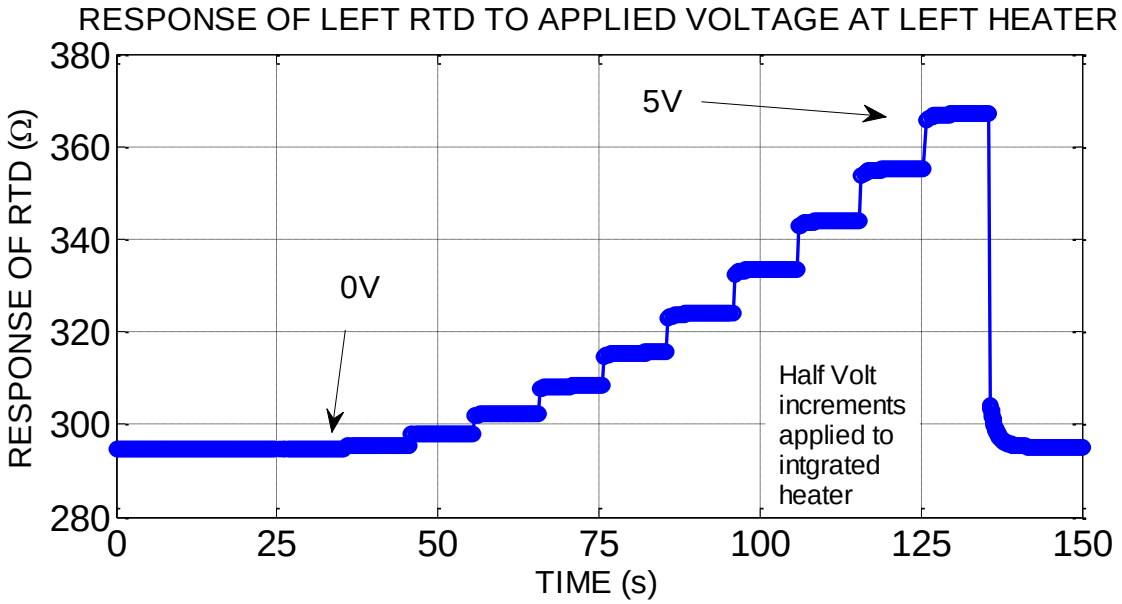

Figure 4.3-2. Response of left chamber RTD to heater.

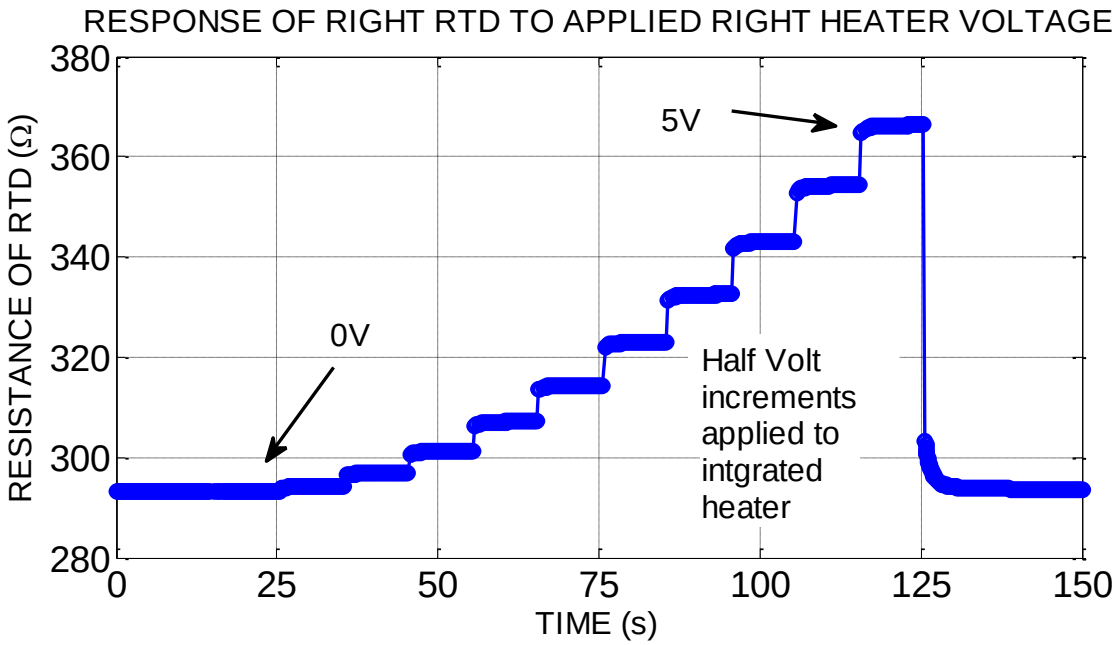

Figure 4.3-3. Response of right chamber RTD to heater.

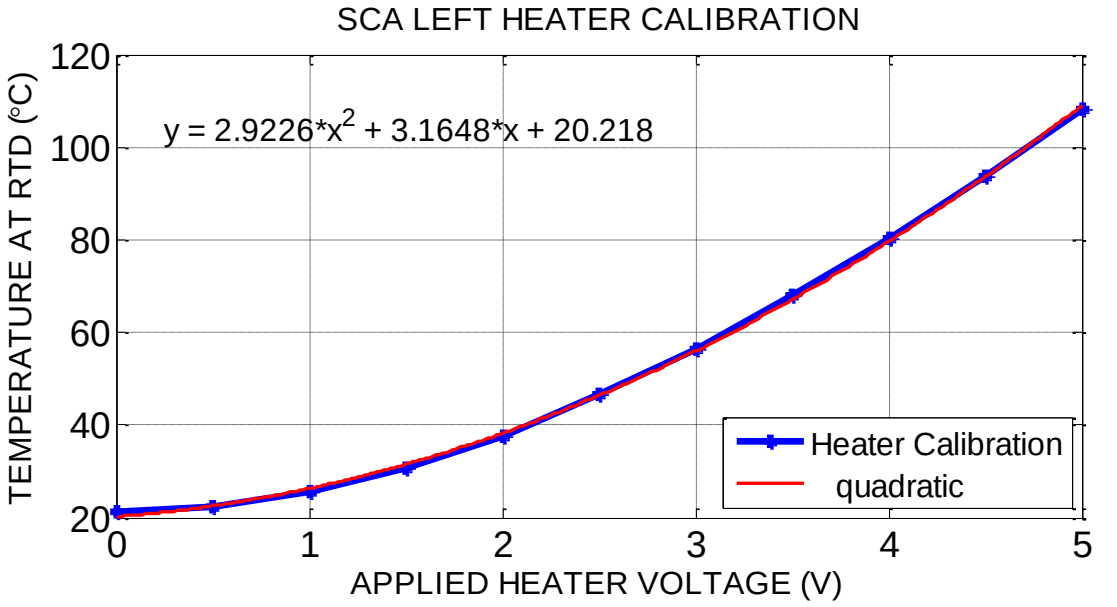

Figure 4.3-4. Temperature of left chamber for applied heater voltage.

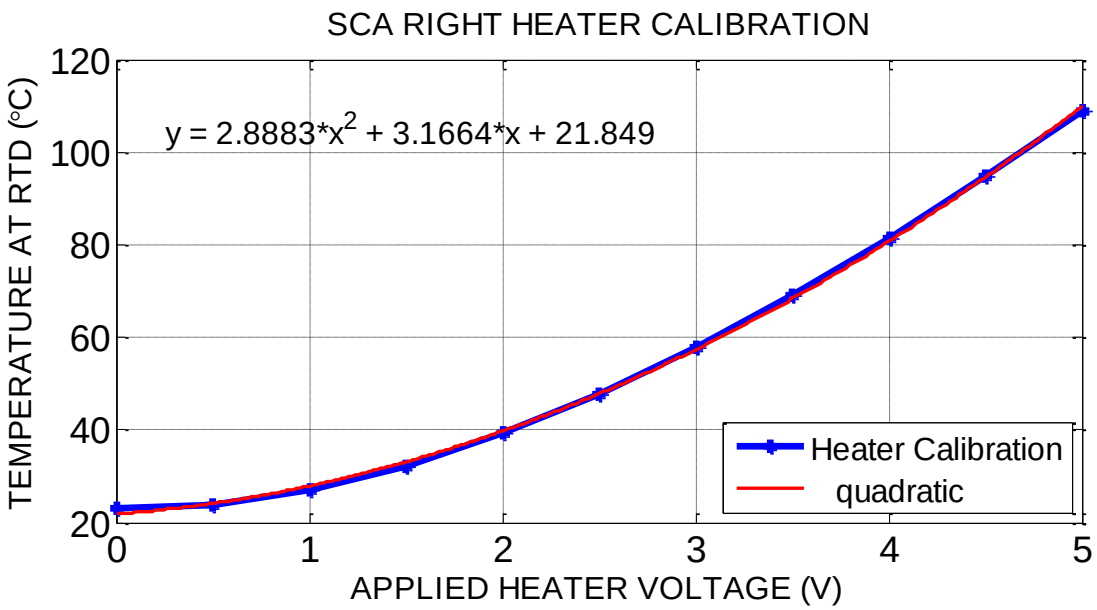

Figure 4.3-5. Temperature of right chamber for applied heater voltage.

4.4 Sensitivity

One figure of merit for the operation of the device is its sensitivity. The sensitivity is the amount of resistance change for a given change of temperature. A high sensitivity of the RTD is a critical factor for the ability to detect small temperature values. The sensitivity is obtained from the slope of the calibration curve as shown in figure 4.4-1. In figure 4.4-2, a device shows the detection of approximate 0.06ºC change in temperature due the illumination of the RTD with an incandescent light.

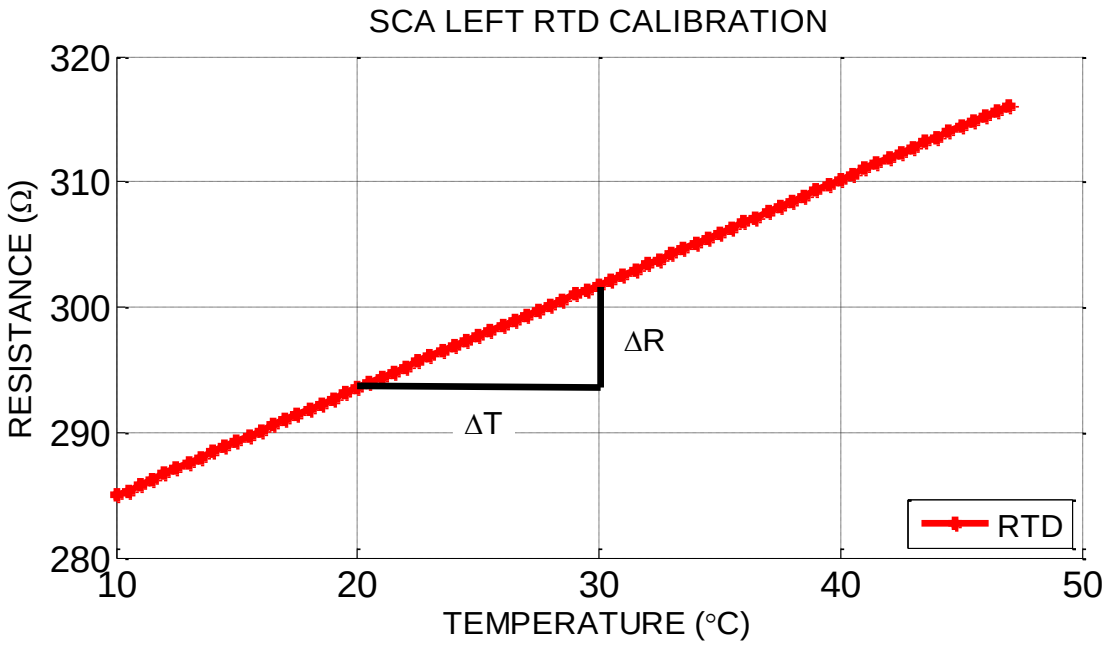

Figure 4.4-1. Sensitivity obtained from the slope of the calibration curve.

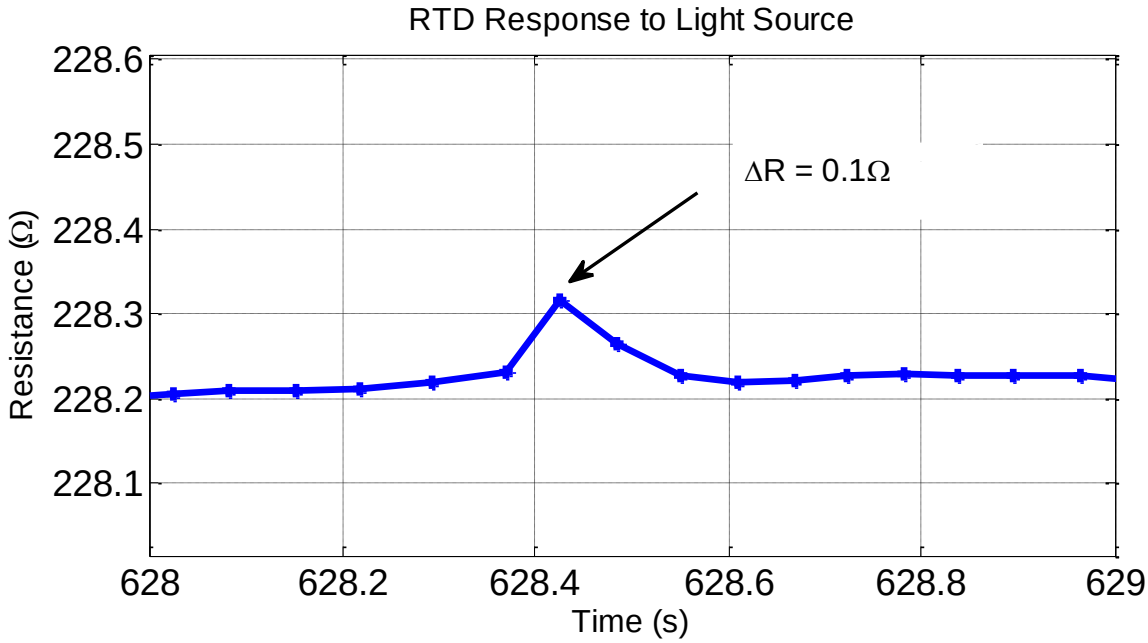

Figure 4.4-2 Response of RTD to incandescent light source showing sensitivity to detect less than a 0.1Ω change. This change corresponds to a change if 0.06°C.

The following table lists the sensitivities obtained through the slope of the calibration curve and through the linear fit equation of the calibration curve for the devices used to perform the metabolism monitoring experiments.

Device	ΔT (ºC)	ΔR (Ω)	Sensitivity (Calculated) (Ω/ºC)	$R_0\alpha$ (Fitted) (Ω/ºC)
SCA Left RTD	8.3	10	.8300	.8362
SCA Right RTD	8.5	10	.8500	.8491
SS2-C Left RTD	10	5.6	.5600	0.5501
SS2-C Right RTD	10	5.6	.5600	0.5501

Table 4.4-1. Sensitivities for selected devices used during metabolism experiments.

4.5 Step Response

Additional parameters of interest to the performance of the DSC include the thermal mass, thermal resistance, and equilibrium time constant. To experimentally determine these parameters a step response measurement is performed. To apply the step response, the device is connected in the same configuration as for the heater calibration, recall figure 4.3-1. LabView is used to control the power supply to apply a fixed magnitude step power input with fixed duration, shown in Figure 4.14.

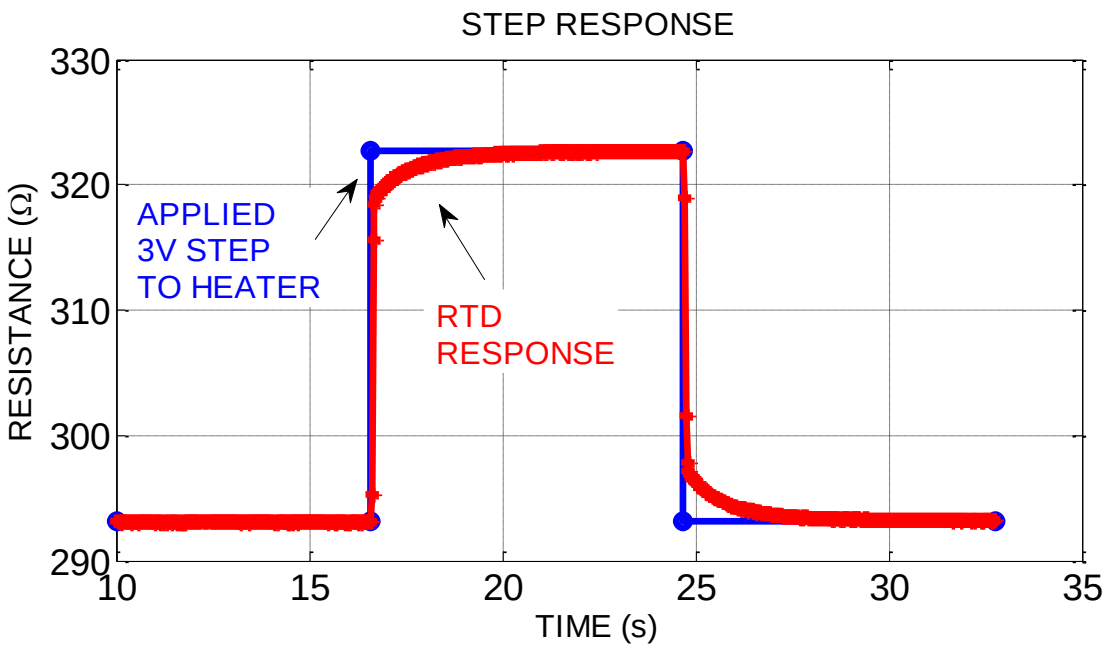

Figure 4.5-1. Step response of SCA RTD to applied step input.

The time constant, τ, is the time required for the step response to reach 63% of its steady state value. The thermal mass can be expressed as a thermal capacitance, and its value is related to the slope of the step response curve at t=0[24]. The thermal resistance is a function of the steady state temperature value and the power input[24]. The equations are shown below, and a plot of the response and the thermal parameters are shown in figure 4.5-2.

$$\Delta T(t) = P_{in} R_t \cdot [1 - e^{\left(\frac{-t}{\tau}\right)}] \quad (^{\circ}C) \tag{4.6}$$

$$\Delta T(t = \tau) = \Delta T_{ss}\{1 - e^{(\frac{-\tau}{\tau})}\} = \Delta T_{ss} \cdot 0.63 \quad (^{\circ}C) \tag{4.7}$$

$$C_{th} = P_{in} \cdot \left[\frac{d\Delta T}{dt}|_{t=0}\right]^{-1} \quad \left(\frac{J}{^{\circ}C}\right) \tag{4.8}$$

$$R_{th} = \frac{\Delta T_{ss}}{P_{in}} \qquad \left(\frac{^{\circ}C}{W}\right) \qquad (4.9)$$

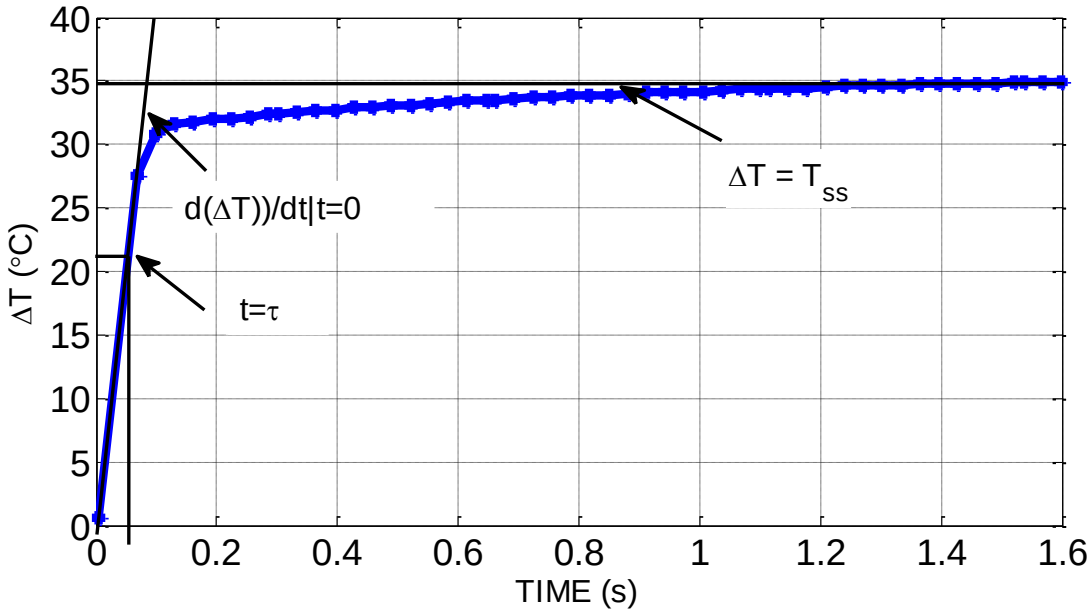

Figure 4.5-2. Thermal properties extracted from the step response.

When the power to the heater is switched off, the DSC will cool to ambient conditions. The cooling of the device will have the same time constant as for the heating case. The results from the experiment can be fitted using the equation:

$$f(x) = \alpha[1 - e^{-\beta x}] \qquad (4.10)$$

Where the coefficients α and β correspond to the steady state temperature and $1/\tau$ respectively. From here we can determine the thermal capacitance from equation 4.8 and thermal resistance by dividing the steady state temperature by the applied power. The results of step response analysis for the devices used in these experiments are shown in table 4.5-1. The results were obtained with an empty device in ambient atmosphere conditions and are comparable to similar published devices[24].

Device	ΔT (ºC)	Pin (W)	d(ΔT)/dt, t=0	Thermal Resistance R_{th} (ºC/W)	Thermal Capacitance C_{th} (J/ºC)
SCA	34.81	0.01166	1035	2984.69	1.126E-5
SS2-C	82.82	0.05923	1259	1398.23	4.704E-5

Table 4.5-1. Thermal properties of devices used for metabolism monitoring experiments.

4.6 Noise Performance

The small resistance fluctuations that arise from within the RTD sensor are classified as inherent noise. This inherent noise can be problematic because the fluctuations will be reflected to the temperature reading and limit its ability to resolve small values. The noise is called Johnson noise and is caused by physical mechanisms such as the thermal excitation of the moving charge carriers in a resistor[16]. These moving charge carriers are temperature dependent and the noise power in turn is also temperature dependent[16].

The mean square value of noise voltage is calculated as:

$$\bar{V}_n^2 = 4kTR\Delta f \qquad (4.11)$$

Where k is Boltzmann's constant, T is the temperature (K), R the resistance (Ω) and Δf the frequency bandwidth in Hz over the measurement range, in this case Δf = 1Hz. As the relationship shows, an increase in either the temperature or base resistance will increase the noise in the sensor. Figure 4.6-1 shows the effective of signal noise on the detectable signal. For a signal to be interpreted, the magnitude should be approximately twice the magnitude of the fluctuations.

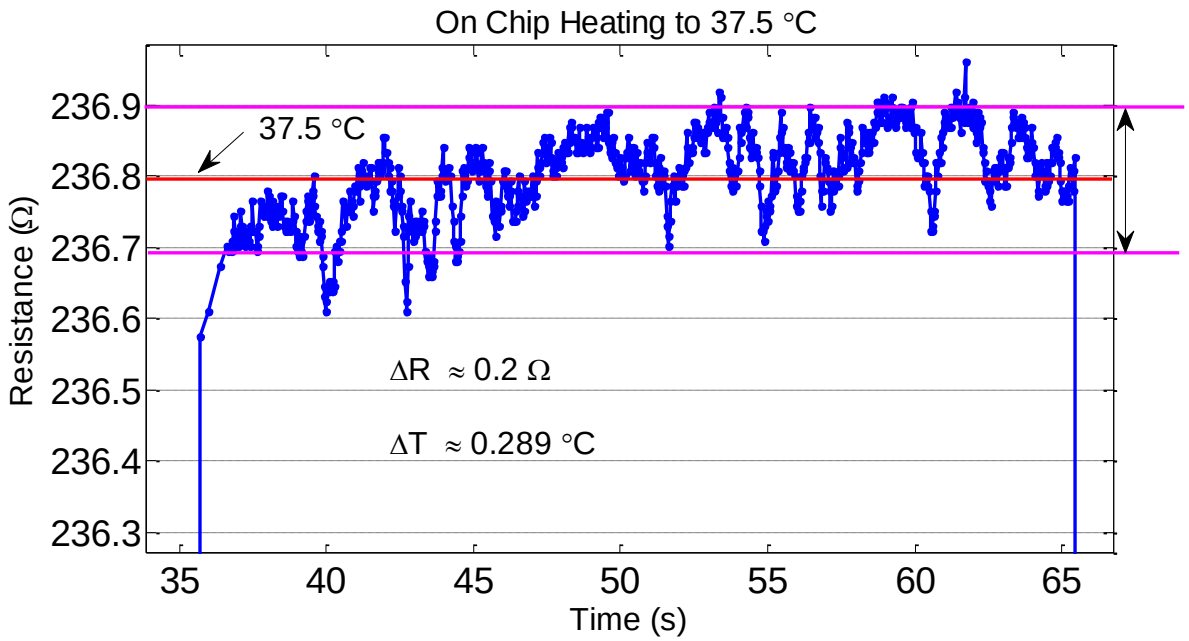

Figure 4.6-1. Sensor noise during heating limits the detectable signal.

An additional source of noise that should be considered is interference or transmitted noise, which is picked up from outside the sensor system[16]. The specific mechanism which affects the sensors detection ability is changes in ambient temperature[16]. This interference is classified as additive and affects the sensing element by mixing with the intended signal and propagating to the output[16].

$$R_{out} = R_s + R_n \quad (\Omega) \qquad (4.12)$$

Additive noise is independent of the output signal and does not change in magnitude when the signal changes due to the linearity of the sensor[16]. It is even present when the output signal is zero.

One method to increase the stability against additive noise is to operate them in a differential configuration. With this technique, sensors are operated in pairs, one for the sensing signal and one for a reference signal. The output signals are then subtracted from

each other. When both sensors are subjected to identical transmitted common mode noise the subtraction eliminates the noise. The quality of the noise rejection is defined by a number called the common-mode rejection ratio (CMRR)[16].

$$CMRR = 0.5\frac{S_1 + S_0}{S_1 - S_0} \qquad (4.13)$$

Where S_1 represents the main sensor signals output, and S_0 represents the reference sensor signals output[16]. The CMRR can also be defined as a measure of the sensors symmetry[16]. To be effective as a means to eliminate noise, the sensors must be placed as close together as possible, be identical and subjected to the same environment[16].

An example of the effect of common-mode noise reject thru the use of differential techniques is shown next. Figure 4.6-2 shows the response of the main or sample sensor, while figure 4.6-3 shows the reference sensor. The difference of the two outputs is shown in figure 4.6-4; it shows the reduction or elimination of the common mode noise.

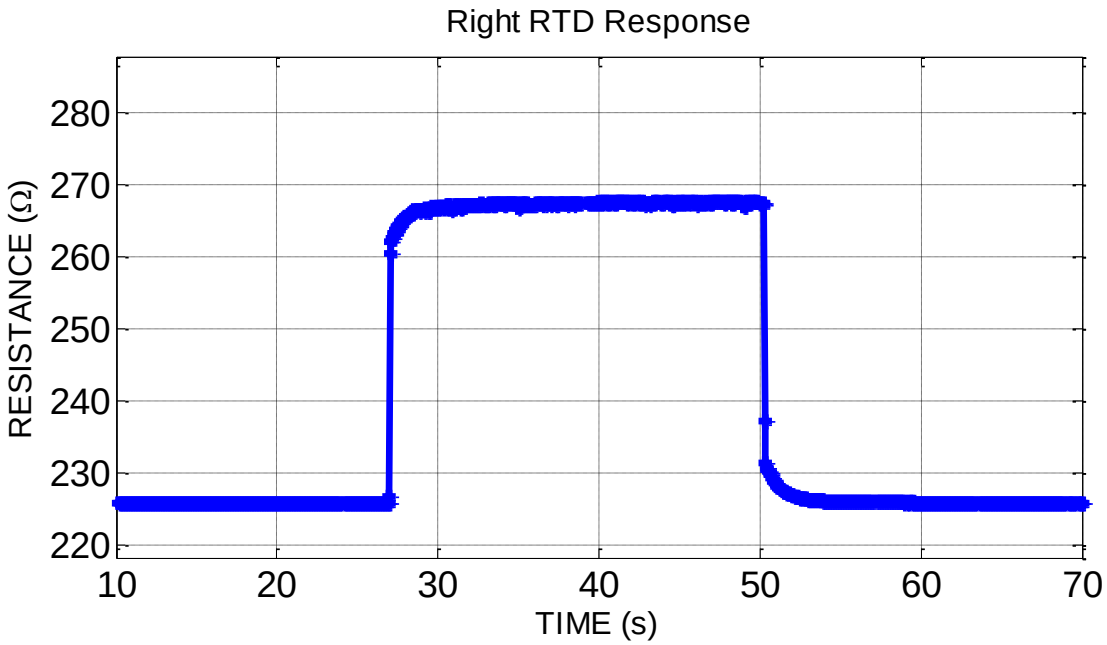

Figure 4.6-2. Example of sample sensor response without noise.

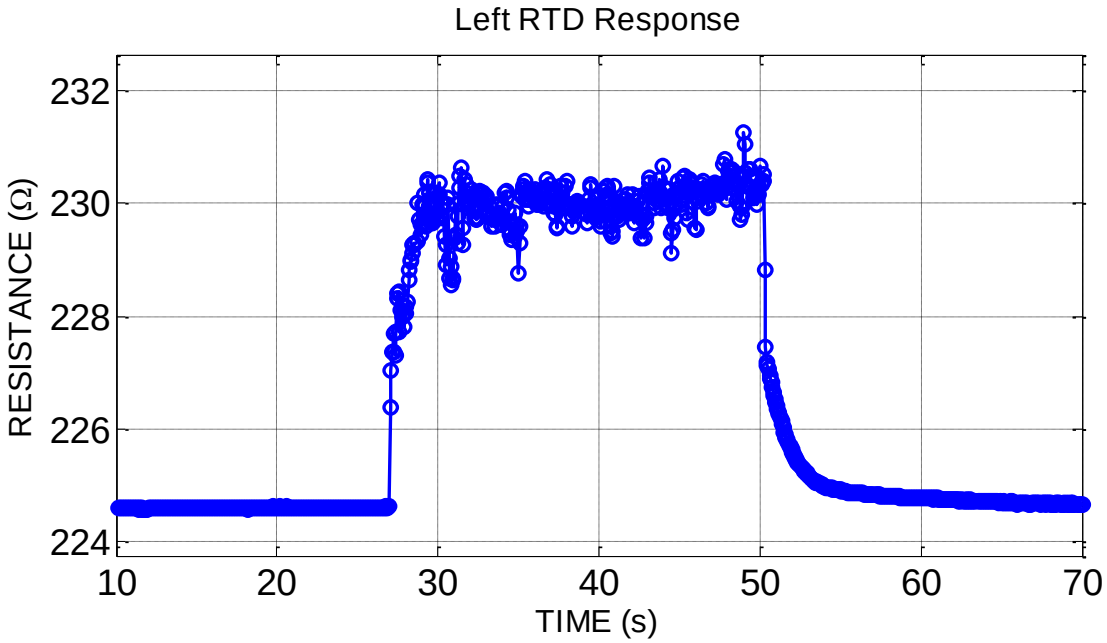

Figure 4.6-3. Example of reference sensor response with noise present in the signal.

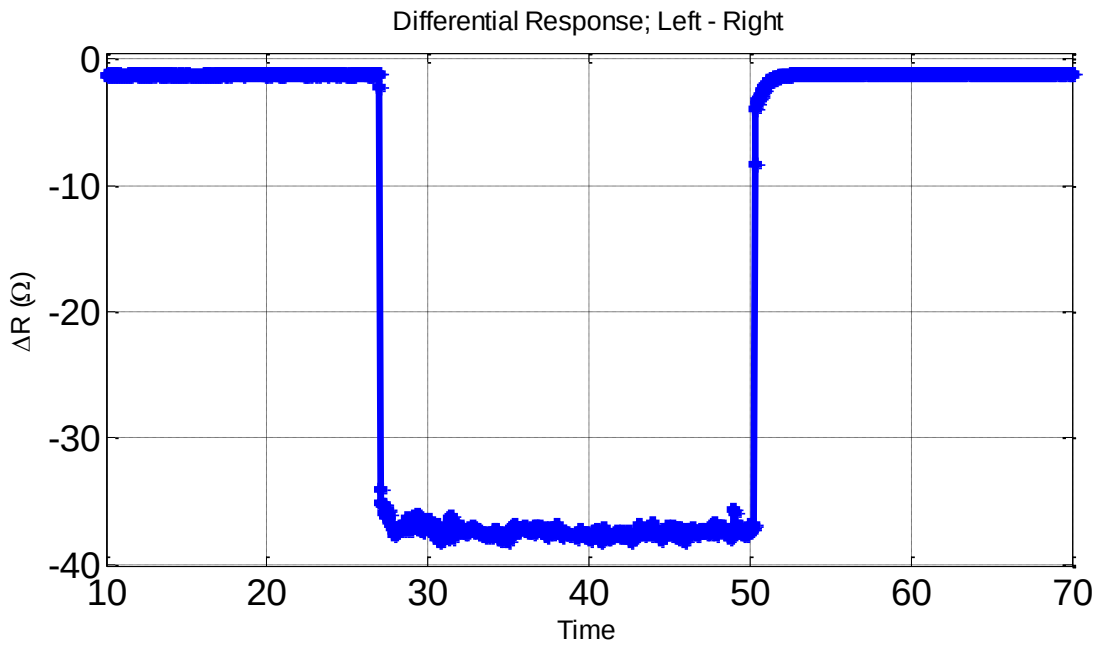

Figure 4.6-4. Differential response showing reduction of noise.

5 DSC Experiments

With the devices fabricated, mounted to a chip carrier, and calibrated, the testing of cellular samples can begin. Tests were performed at North Carolina State University's department of biomedical engineering under the guidance of Dr. Glenn Walker. The metabolism of two different cell lines was observed, JM-1 liver cancer cells and lymphocytes. This section will discuss the experiments and some initial results.

5.1 DSC SCA Baseline Experiments

The setup for testing began by performing some initial characterization of the DSC with cell culture medium to become familiar with the response of heater and RTD. The devices were loaded from the backside with 10µl of Bovine Serum Albumin (BSA) cell culture medium covering the entire membrane and a layer of mineral oil to prevent evaporation as figure 5.1-1 shows. The test equipment was comprised of an Agilent power supply for both integrated heaters and an Agilent multimeter for each RTD. All equipment was controlled with a computer running Labview.

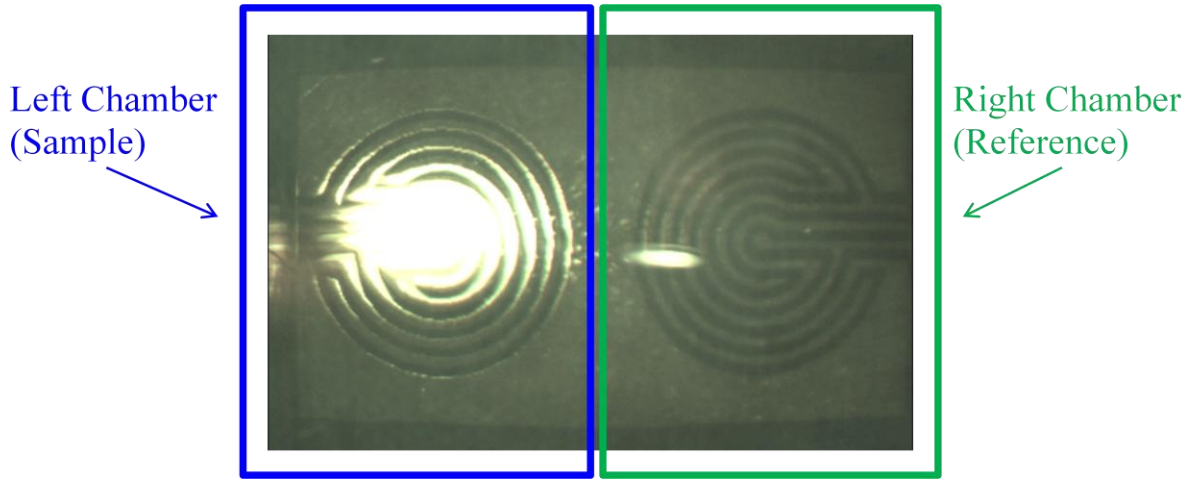

Figure 5.1-1. Cell culture medium on sample and reference chamber.

Electric current was applied to each of the integrated heaters and the temperature of each chamber was recorded by the RTDs. This test allowed us to know exactly how much current should be applied to the heater to achieve a 37ºC environment for each chamber. It also gave us the inherent behavior of the device. Although the devices are designed to be identical, non-uniformities in the metal evaporation or liftoff procedure could be reflected as differences in the device. By performing this test we effectively created a baseline response for the device that could be used as a reference for future tests.

Voltage was applied to the heaters for 3 minutes. The plots show that the two RTDs are nearly equal in their response, as shown by figure 5.1-2. The differential was obtained by subtracting the left chamber data from the right chamber data. If the devices have been fabricated to be identical, then the differential of the two RTDs should show no response. The plot in figure 5.1-3 confirms that they are nearly identical.

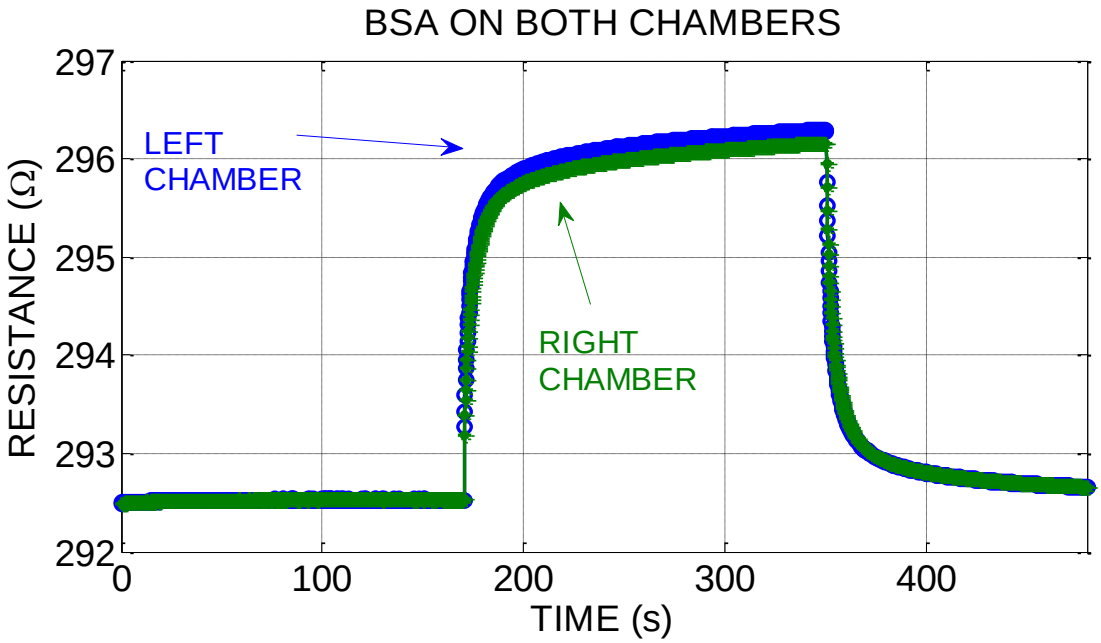

Figure 5.1-2. DSC SCA baseline calibration with BSA cell culture medium.

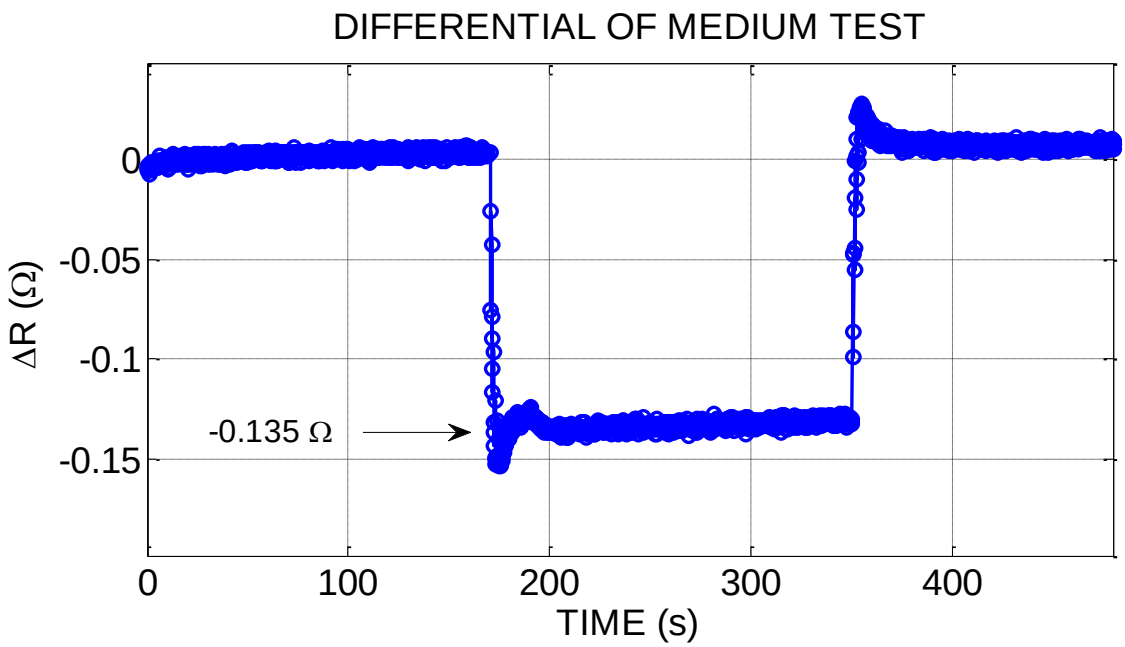

Figure 5.1-3. DSC SCA differential of baseline calibration with cell culture medium.

5.2 DSC SCA Experiments With JM-1 Liver Cancer Cells

Cellular metabolism monitoring experiments were performed by loading cell culture medium on one chamber and cell culture medium with cells on the other chamber, then covering the entire DSC with mineral oil. Based on the previous setup experiments, we re-applied the voltage required to achieve 37ºC for each chamber while measuring the temperature over time. We operated under the hypothesis that the chamber with cells will have a slightly higher temperature due to the heat produced by the cells.

The same device used in the previous experiment was used to perform the following experiment after cleaning with isopropyl alcohol (IPA) and flushing with de-ionized water (DI) followed by N_2 dry. It was conducted with approximately 4µl cell

culture medium containing JM-1 liver cancer cells loaded onto the left chamber, while the right chamber was loaded with only cell medium, as shown by figure 5.2-1.

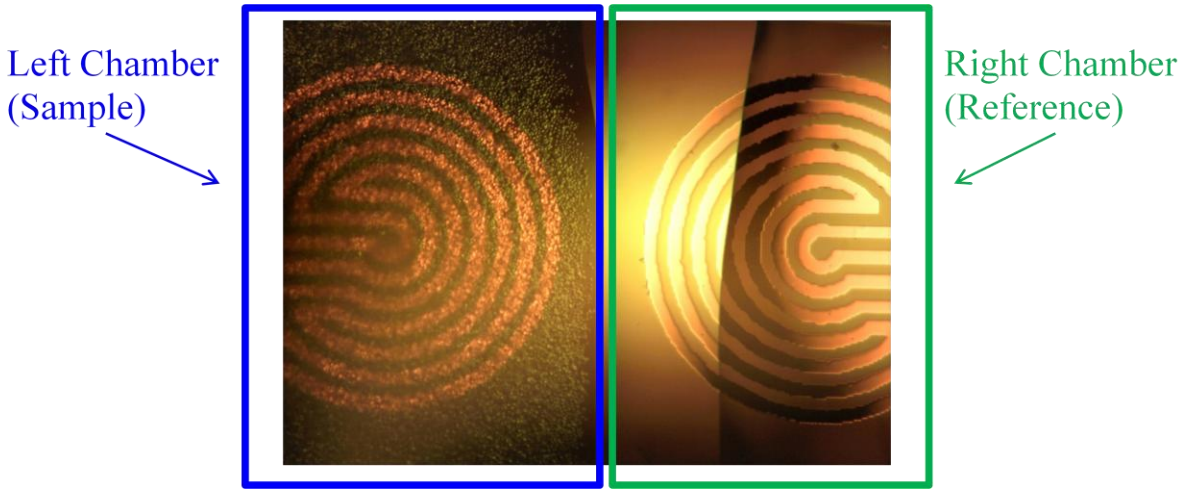

Figure 5.2-1. Cell culture medium with liver cancer cells loaded onto the left chamber, cell culture medium only loaded onto the right chamber. Both covered with mineral oil.

The DSC was reconnected to the test equipment, Agilent power supply for both integrated heaters and an Agilent multimeter for each RTD. All equipment was controlled with a computer running Labview. The DSC and samples were allowed sufficient time to equilibrate with the room temperature before beginning the experiment. The same value for the heater voltage used in the previous experiment was re-applied to the heaters for three minutes and the RTDs' responses were monitored. The results are shown in figure 5.2-2. The differential was obtained by subtracting the right chamber data from the left chamber data. The differential plot is shown in figure 5.2-3.

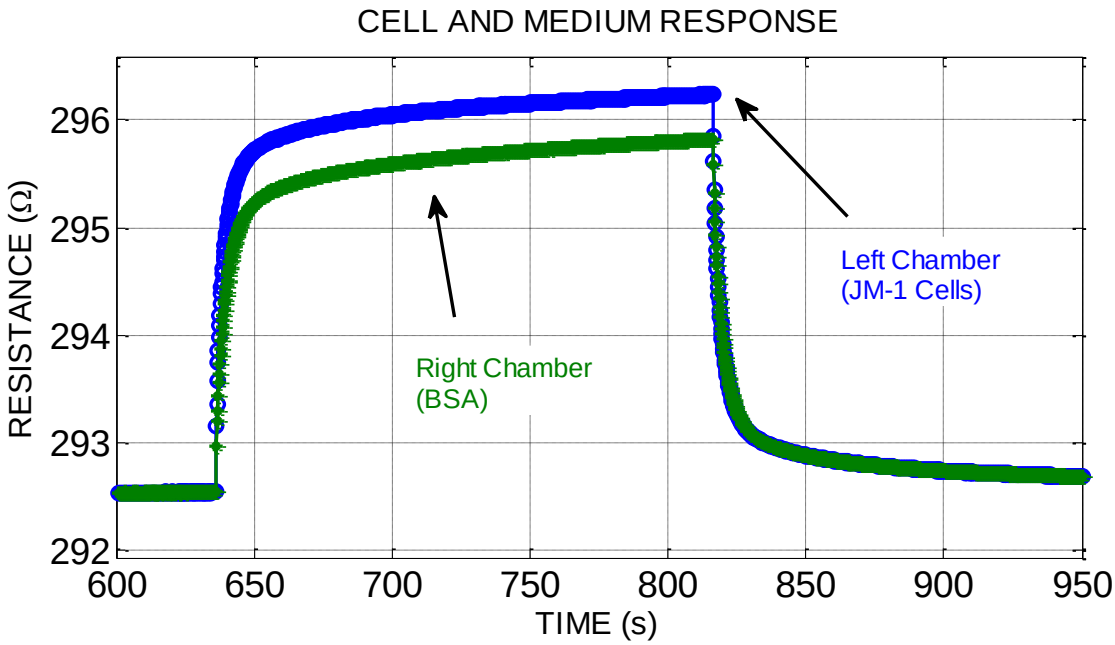

Figure 5.2-2. Response of RTDs. Cell culture medium with JM-1 cells on left chamber, while cell culture medium only on right chamber.

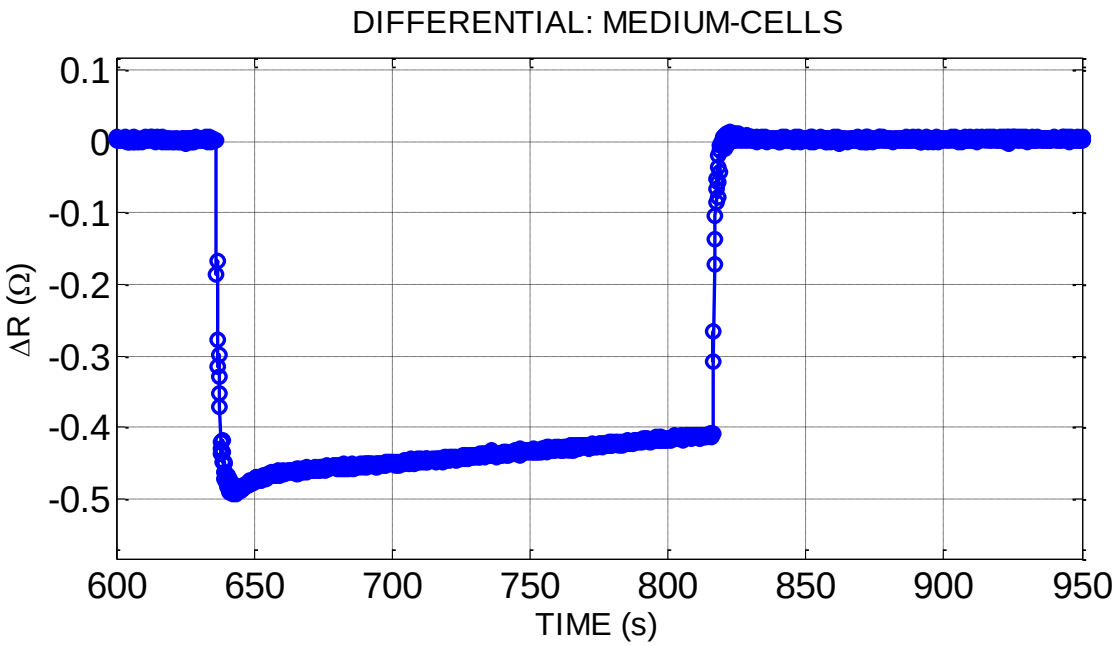

Figure 5.2-3. Differential response. Cell culture data subtracted from JM-1 cell data.

The comparison of the differential response from the two separate experiments is shown in figure 5.2-4. The next step is to subtract the base line differential response from the cell monitoring experiment differential response. This will give the actual contribution from the addition of the cells because the response that is obtained from the first experiment will still contribute to the response of the cell based experiments.

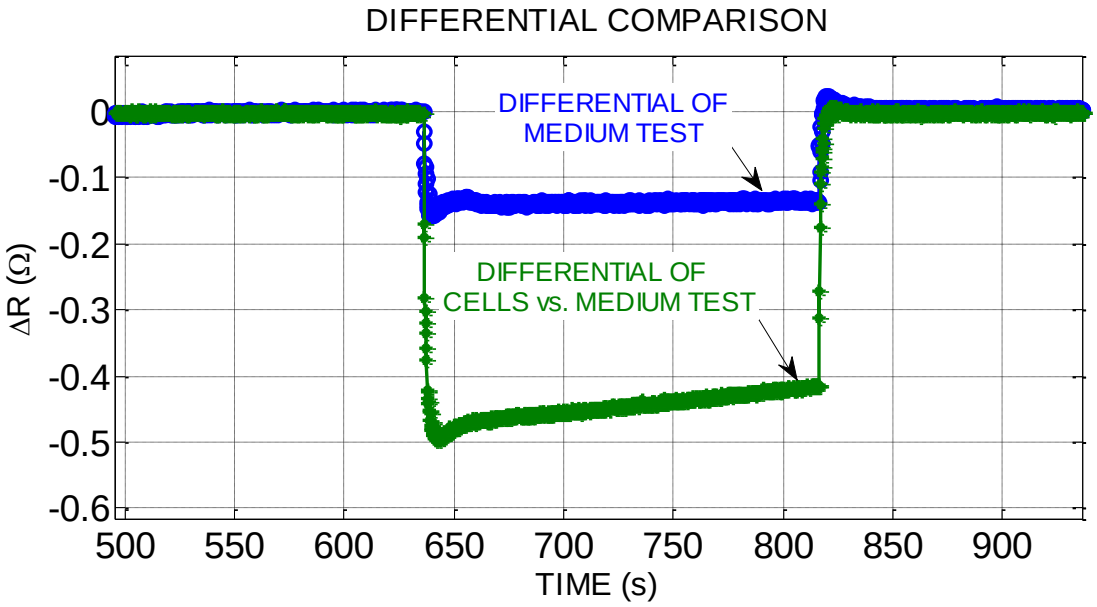

Figure 5.2-4. Comparison of the differential responses from each experiment.

The calculations to determine the temperature contribution from the addition of the cells is as follows. First we begin with a general calibration equation for each plot:

$$R(T_1) = R_{0_1}(1 + \alpha_1 T_1)$$
$$R(T_2) = R_{0_2}(1 + \alpha_2 T_2)$$

Next subtract one from the other:

$$R(T_1) - R(T_2) = R_{0_1} - R_{0_2} + R_{0_1}\alpha_1 T_1 - R_{0_2}\alpha_2 T_2$$

Then the following assumptions are made which hold true due the fact that the same device was used for each experiment:

$$\textit{if } R_{0_1} = R_{0_2} \textit{ and } \alpha_1 = \alpha_2$$
$$\textit{then } (R_{0_1} - R_{0_2}) = 0$$
$$\textit{and } (R_{0_1}\alpha_1 T_1 - R_{0_2}\alpha_2 T_2) \rightarrow R_0\alpha(\Delta T_{1-2})$$

Finally we substitute numerical values:

$$\frac{\Delta R(T_{1-2})}{R_0\alpha} = \Delta T_{1-2}$$
$$\frac{0.45\Omega - 0.135\Omega}{0.84\Omega^{\circ}C^{-1}} = 0.375^{\circ}C = \Delta T$$

The values used to determine the contribution were the average over the span of the applied step. If we subtract the baseline response from the cell based experiment, we can see in figure 5.2-5 that over the applied step there is approximately 0.08ºC decrease in temperature.

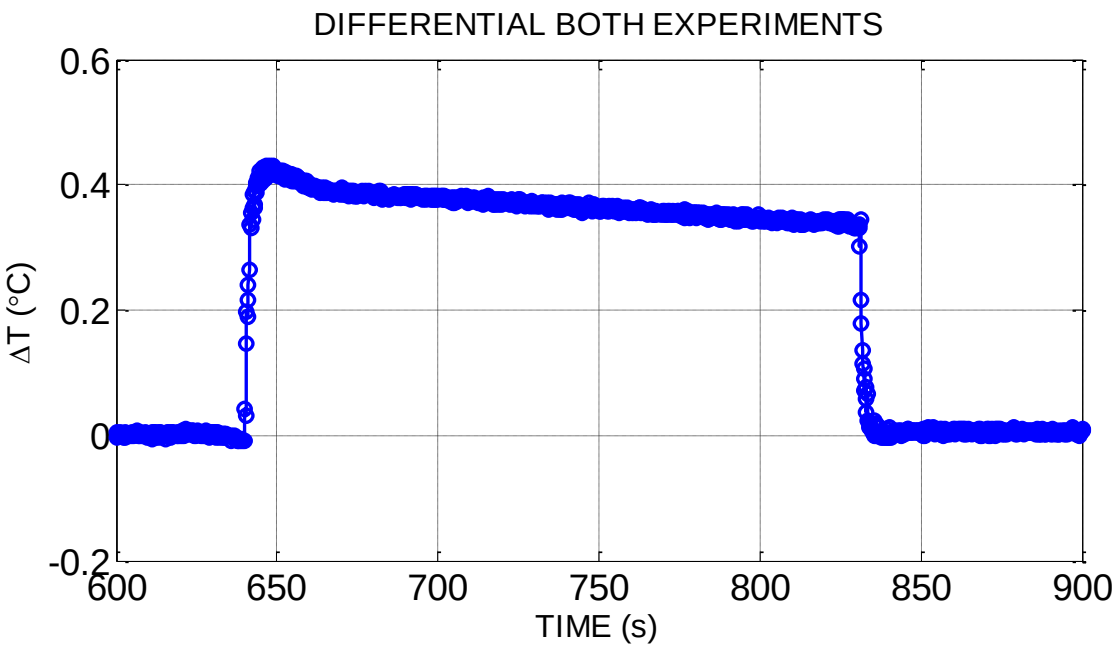

Figure 5.2-5. Temperature contribution due to the addition of JM-1 cells to the cell culture medium.

Our hypothesis for performing these experiments was that the temperature will increase due to the heat production of the cells. Therefore, by the addition of JM-1 liver cancer cells to cell medium we have observed an increase of 0.375ºC over tests performed with only cell medium. Additional analysis of the results and implications of these results in terms of cellular metabolism will be discussed in the next section. Similar experiments as presented previously were performed using normal lymphocytes as a comparison.

5.3 DSC SS2-C Baseline Tests

These tests were performed with a different DSC device, which uses a modified serpentine shape for the RTD and heater segments and is pictured in figure 5.3-1. The same process is followed, the DSC is tested using only cell medium first to determine a baseline response.

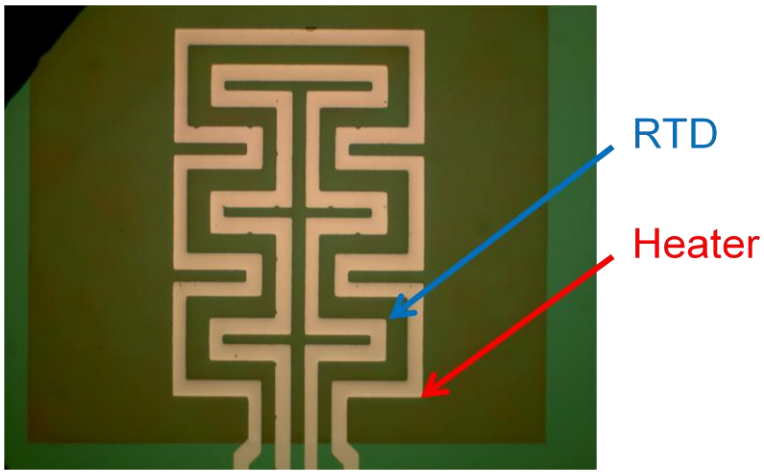

Figure 5.3-1. Geometry of device used for lymphocyte cell experiments.

Again, the DSC was loaded from the backside with 10µl of BSA cell culture medium and covered with mineral oil. An electric current was applied to the heaters to warm the chambers up to 37ºC, while the RTDs response was monitored. That response is shown in figure 5.3-2. Like the previous experiment, the differential showed behavior inherent to this particular DSC device, and the two RTDs are nearly equal, as shown in figure 5.3-3.

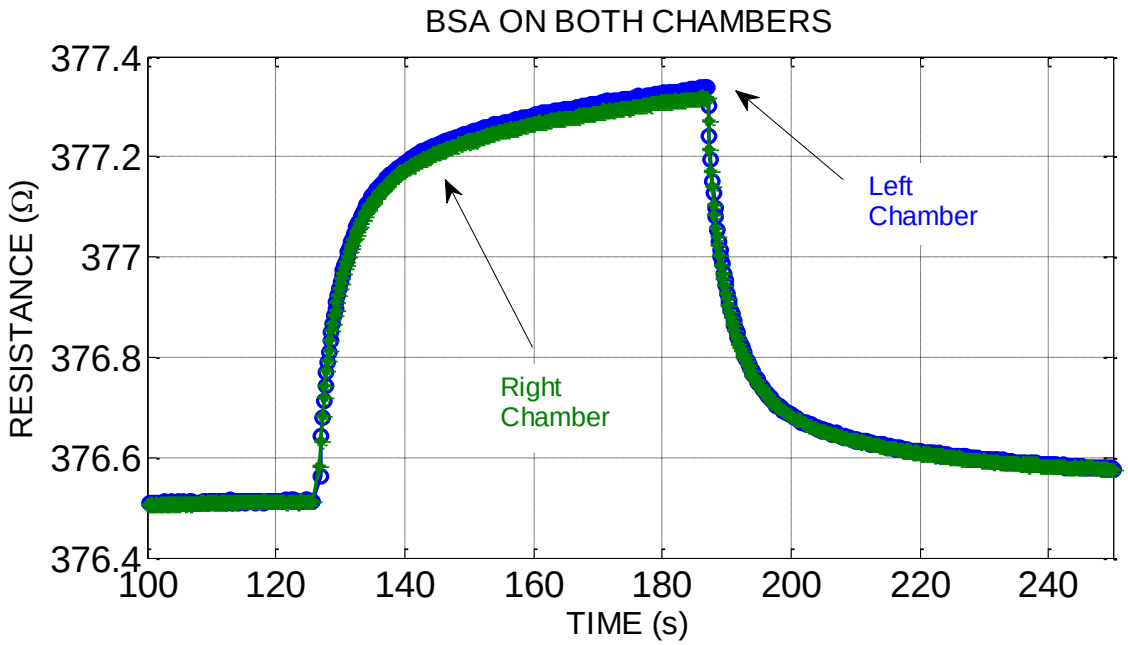

Figure 5.3-2. Response of cell culture medium-only baseline testing.

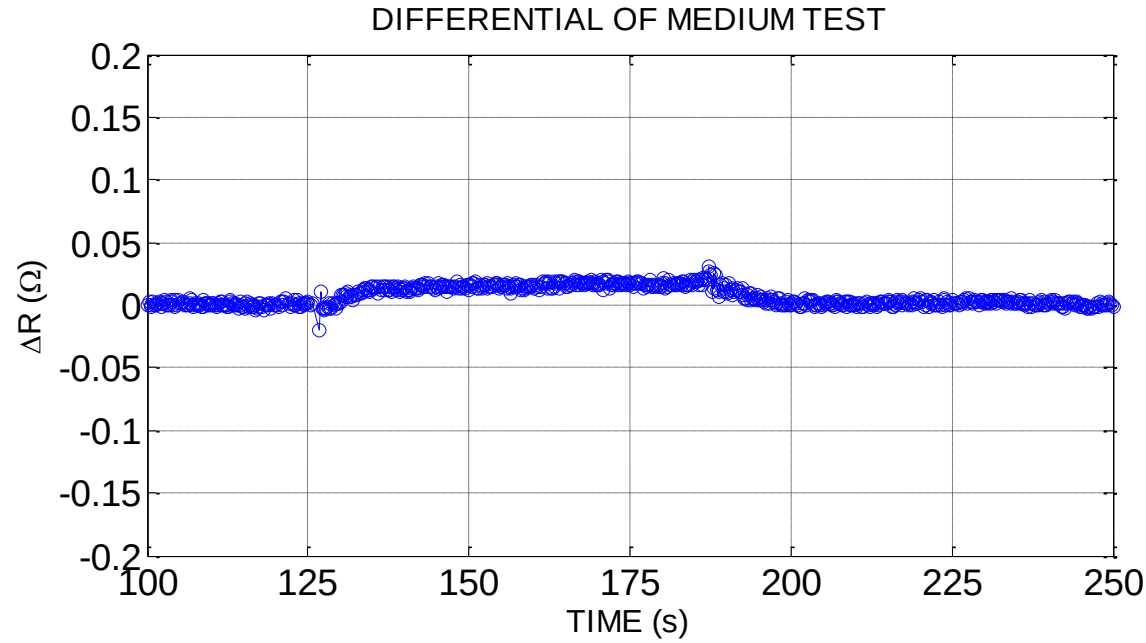

Figure 5.3-3. Differential of cell culture medium baseline testing.

5.4 DSC SS2-C Lymphocyte Cell Testing

The second experiment performed with this DSC was testing normal white blood cells. 4µl of medium containing the cells was loaded onto one chamber while 4µl of cell culture medium only was loaded to the other chamber, and the entire DSC was covered with mineral oil. Figure 5.4-1 shows the cells loaded onto the DSC.

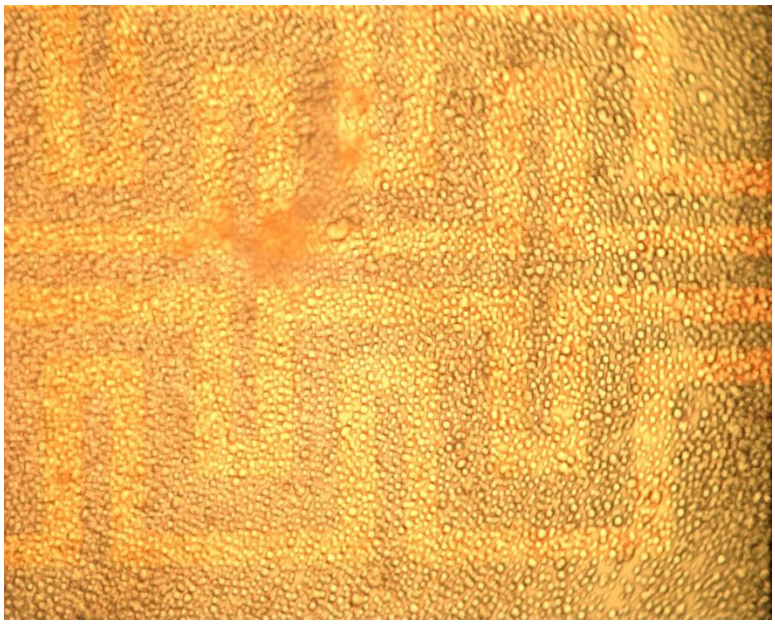

Figure 5.4-1. DSC loaded with normal white blood cells. The RTD and heater traces are the yellow serpentine patterns.

The DSC was reconnected to the test equipment and the voltage required to achieve 37ºC applied. The response of the RTDs was observed to monitor the contribution of added heat due to the presence of the cells. Initial results from testing are shown in figure 5.4-2.

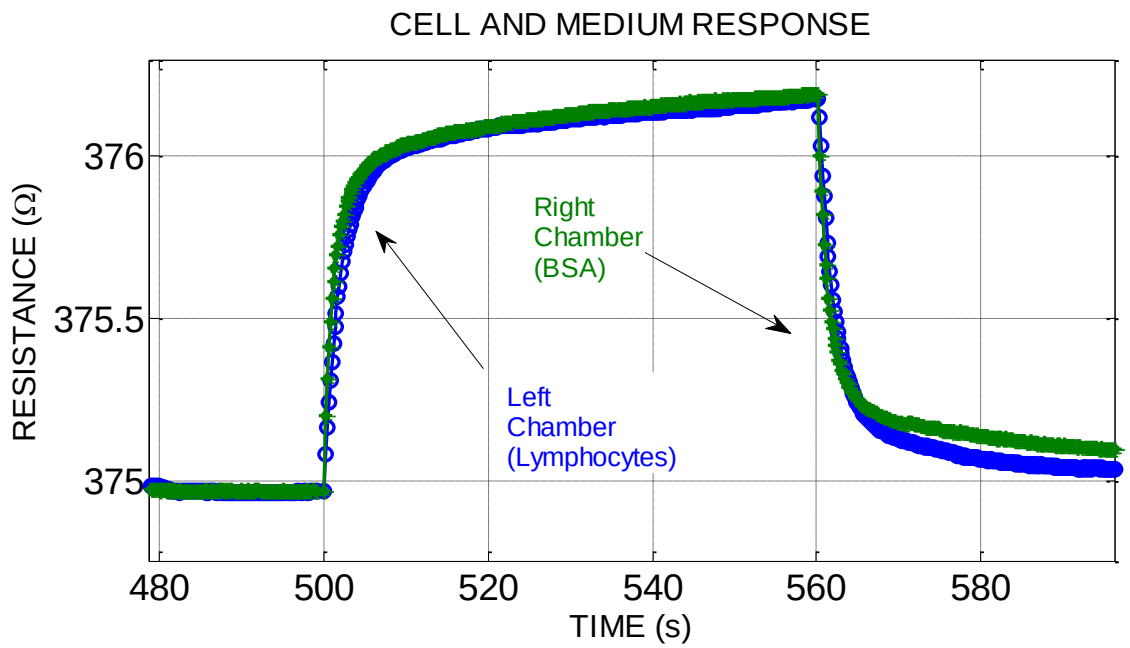

Figure 5.4-2. Response of RTDs. Cell culture medium with lymphocyte cells on left chamber, while cell culture medium only on right chamber.

The differential response shows that after the initial transient responses, there is no apparent difference in temperature between the sample chamber with the cells and the reference chamber without cells, as shown in figure 5.4-3. When the two traces are plotted together in figure 5.4-4 to compare the responses, it is not clear whether a heat contribution from the white blood cells can be observed. Further plotting of differential of the two experiments confirms this as plotted in figure 5.4-5 shows. Because a response is not easily obtained from the raw DSC trace, further analysis of the results is required, including the analysis of the transient response and extraction of the derivative.

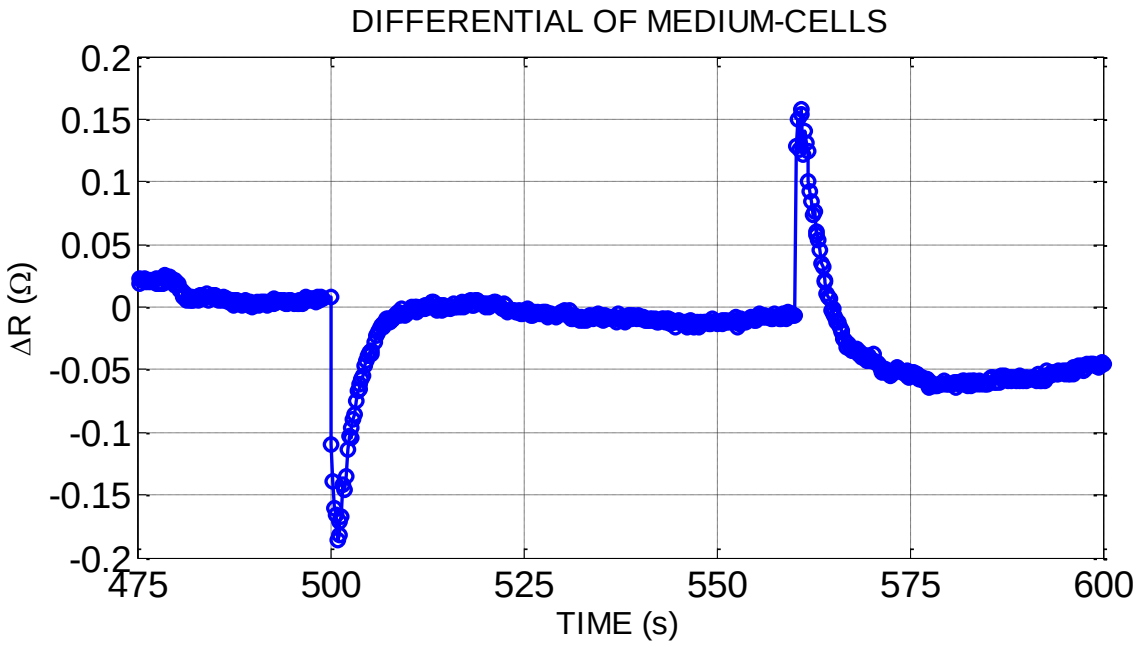

Figure 5.4-3. Differential response. Cell culture data subtracted from Lymphocyte cell data.

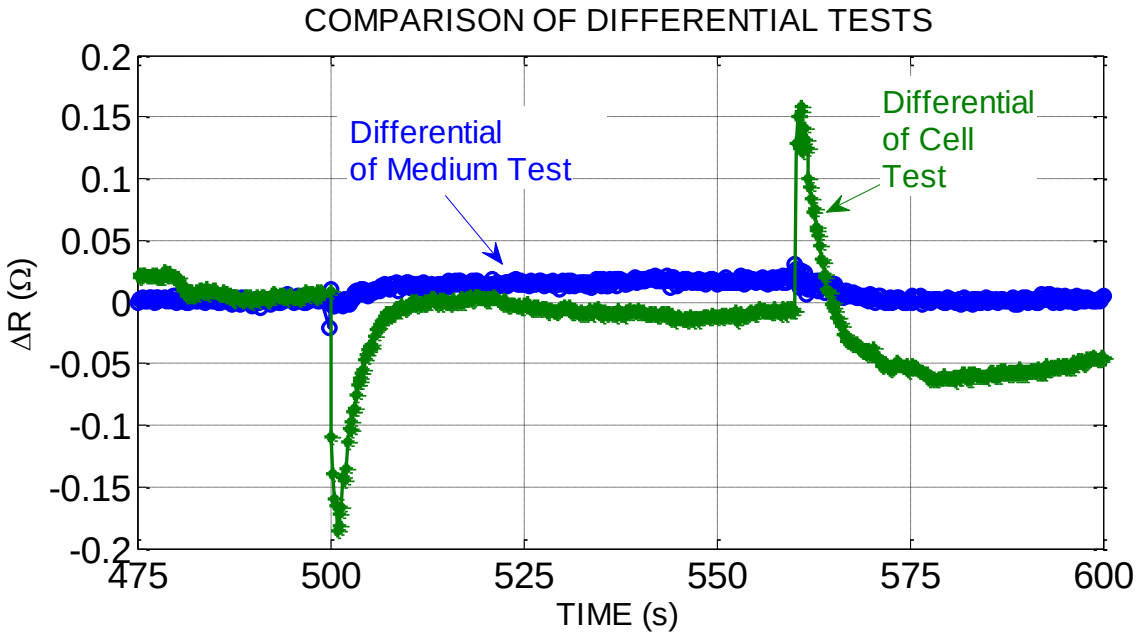

Figure 5.4-4. Direct comparison of the differential responses from each experiment.

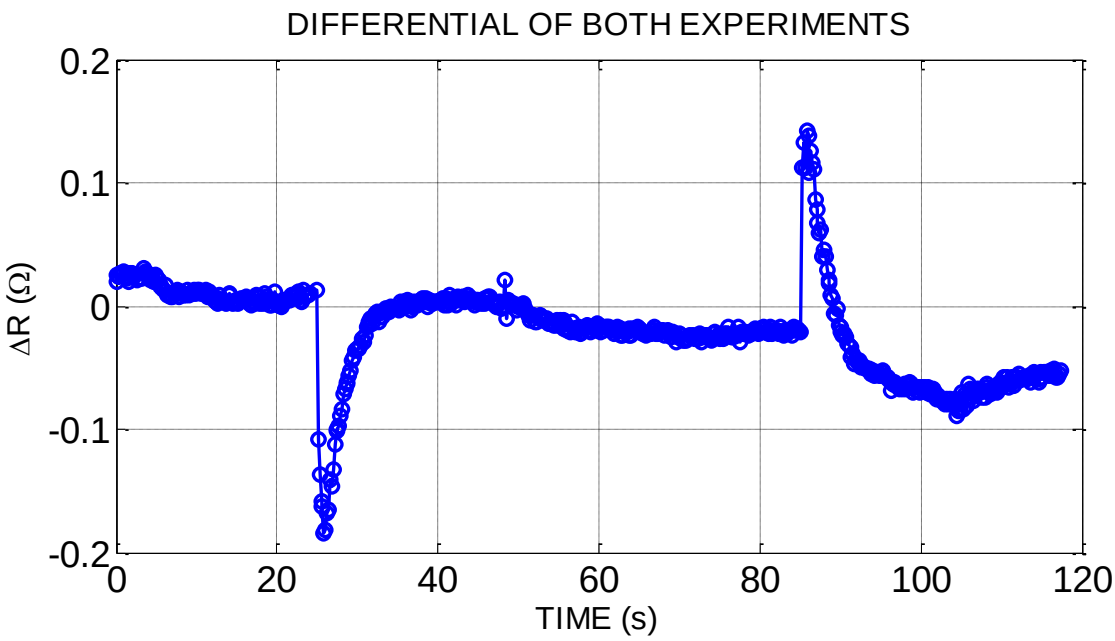

Figure 5.4-5. Differential of lymphocyte differential plot and culture medium differential plot.

5.5 Discussion

The DSC devices were used to monitor cell metabolism to determine their heat power output. Two different cell lines where used: JM-1 cancerous liver cells and normal lymphocytes. Test were performed by first observing only cell medium in both chambers to obtain a baseline response, then cells and medium were loaded into the sample chamber and medium was loaded into the reference chamber. Initial results from the liver cell tests show an average temperature increase of 0.375ºC, while initial results from the lymphocytes are inconclusive. Therefore, additional analysis is required to determine if any heat contribution is present. This analysis will be presented in the next chapter.

6 Analysis of Results

With the cellular sample testing completed, we can turn to analyzing the results of the DSC curves to determine if further information such as the cell heating rate or a means to differentiate between them can be obtained. Two post processing approaches were taken, and both made use of the derivative of the extrapolated temperature curve. One method took the derivative of the raw data curves and then compared them directly, while the other method was to take the differential of the sample cells data against the reference data then obtain the derivative. The results of both methods will be compared in terms of their ability to differentiate the two cell lines.

6.1 Derivative Method One, Direct

For the first method, the raw data obtained from each experiment is curve fitted, and then the 1^{st} derivative is calculated and plotted versus time. To prepare the data for analysis, each heating curve is isolated and time shifted so that zero becomes the start of the step response on the x-axis, and the y-axis is the RTD temperature above ambient (ΔT). Each curve is limited to the first twenty seconds of the response and any remaining response is assumed to be steady state. The reason for this approach is that the fit of the transient portion of the curve is greatly improved and this is where critical information can be obtained from the response about the behavior of the cells.

First, the experiment using the JM-1 liver cancer cell line will be examined. The data is corrected and fit using a sum of two exponential functions in MATLAB. Figure 6.1-1 shows the response and the fitting.

$$y(x) = a(1-e^{-bx})+c(1-e^{-dx}) \qquad (6.1)$$

where x corresponds to time, t; y corresponds to temperature change, ΔT; a & c correspond to partial ΔT steady state; and b & d correspond to partial $\frac{1}{\tau}$.

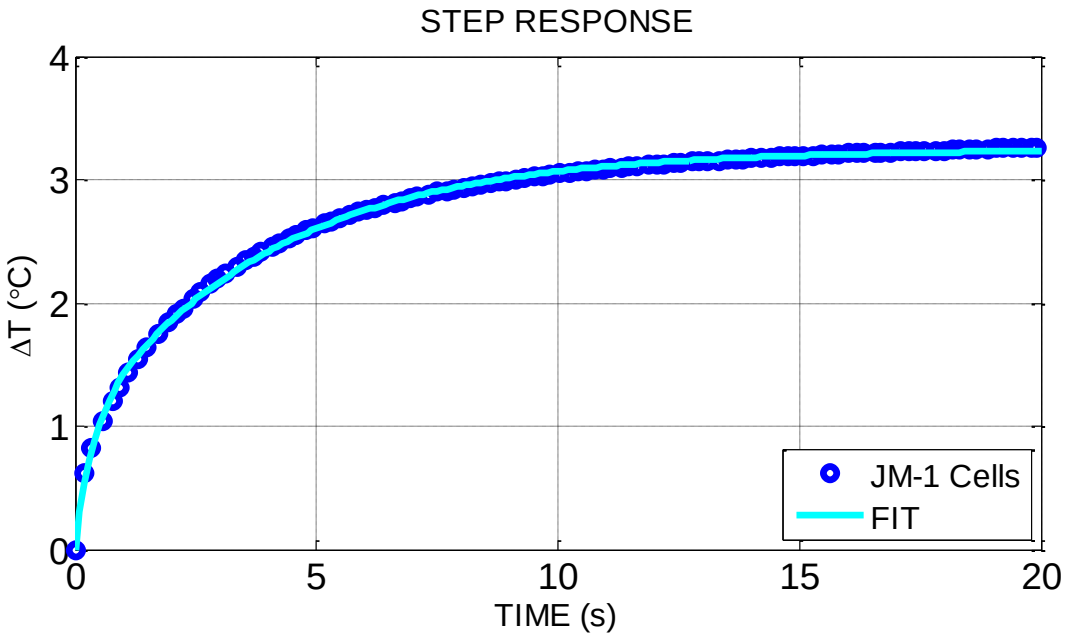

Figure 6.1-1. Heating response of JM-1 cells. Exponential fitting overlaid.

Using MATLAB's curve fitting toolbox, the first derivative is obtained, $\frac{d\Delta T}{dt}$, and plotted versus time, figure 6.1-2.

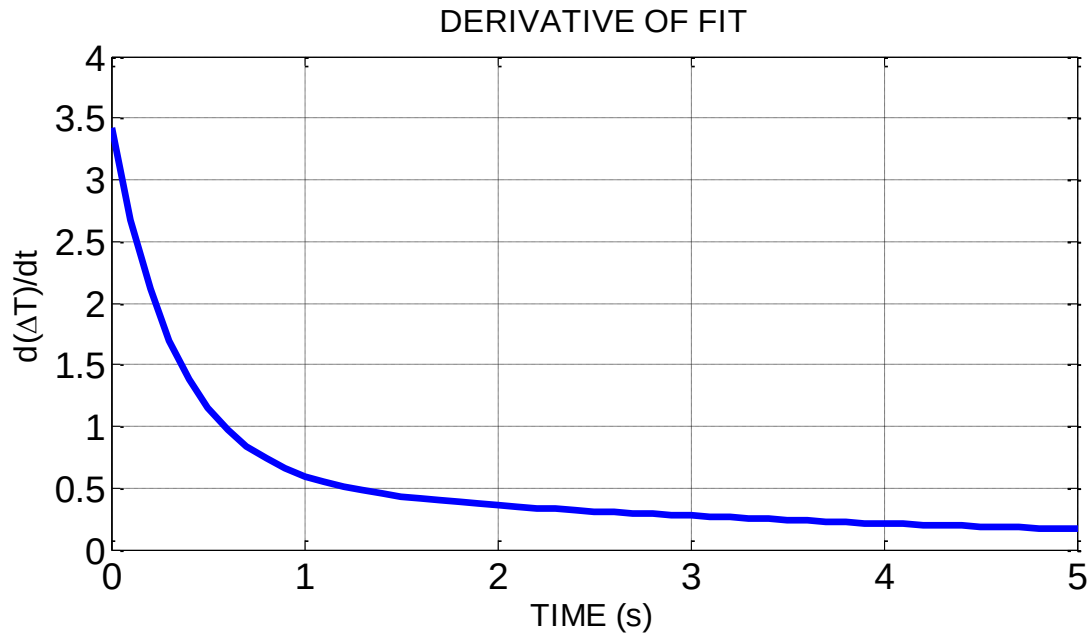

Figure 6.1-2. First derivative of the heating response of JM-1 cells.

The coefficients for the fitting of the step responses shown in figure 6.1-1 and 6.1-3 are given in the following table:

Step Response	a	b	c	d
JM-1	0.6326	2.927	2.155	0.2324
Lymphocytes	0.4405	0.0999	1.637	0.5819

Table 6.1-1. Coefficients for fitting equation.

Next, the experiment containing the lymphocytes is examined; again, the data is corrected and fitted using the same function. The step response is shown in figure 6.1-3.

Using MATLAB's curve fitting toolbox, the first derivative is obtained, $\frac{d\Delta T}{dt}$ and plotted versus time, figure 6.1-4.

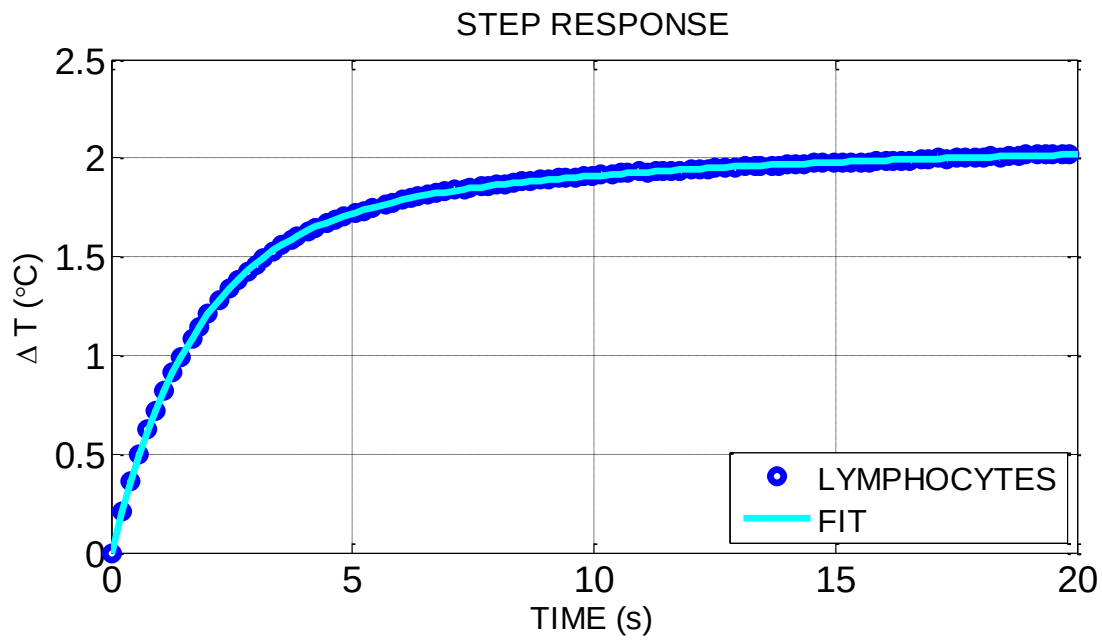

Figure 6.1-3. Heating response of lymphocytes. Exponential fitting overlaid.

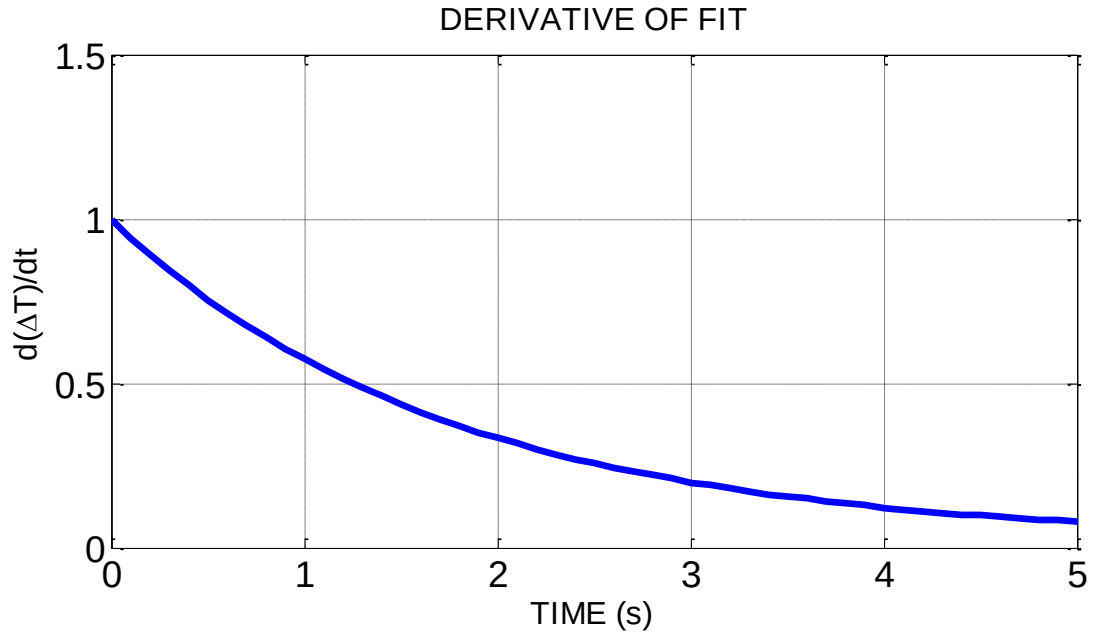

Figure 6.1-4. First derivative of the heating response of lymphocytes.

Recall that inspection of the initial testing results showed that the JM-1 cells potentially added their thermal energy to the system and increased the temperature of sample chamber as compared to the reference chamber. However, the results from the Lymphocyte samples showed no observable increase in temperature above the reference, suggesting that they do not produce enough thermal energy that can be added to the system to be identified. Because of those results, there was not enough information available to make a claim as to identify the cell type based solely on the temperature response. Now we can directly compare the results of the derivative analysis and their implications. Figure 6.1-5 shows that there is an observable difference between the two cells based upon the derivative of the temperature curve. The results of this post processing analysis will allow the identification of different cell types when exposed to a short step power input.

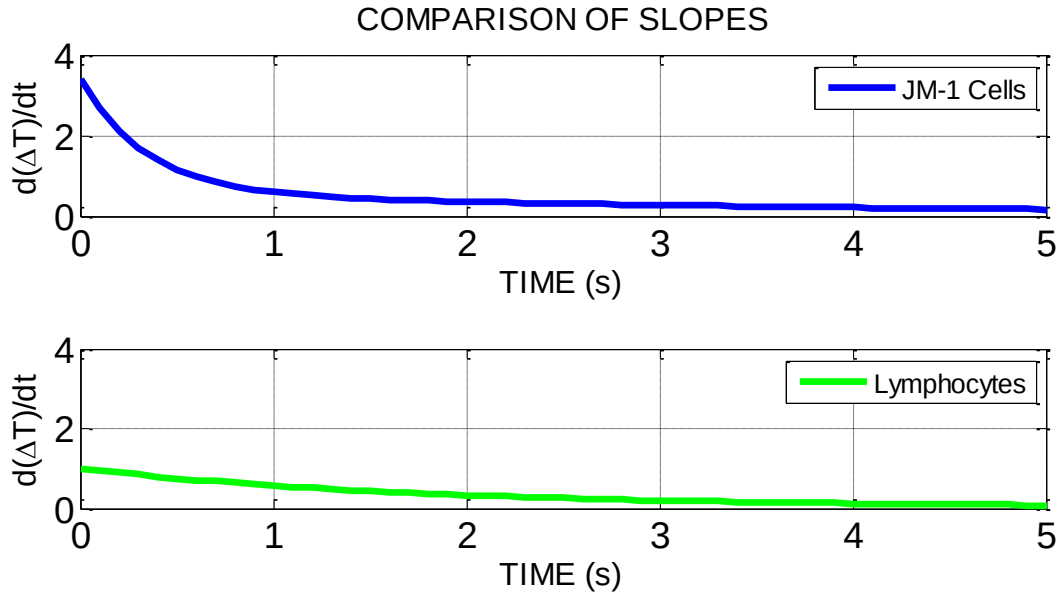

Figure 6.1-5. Comparison of the derivative of the temperature curves for JM-1 cells and lymphocytes.

By using the equation relating thermal energy to thermal mass, we can make a general conclusion on the amount or rate of thermal energy transferred to the system.

$$Q = C_{th}\Delta T \tag{6.2}$$

where Q is the thermal energy transferred, C_{th} is the thermal mass of the system, and ΔT is the change in temperature. However, the value of interest is the amount or rate of thermal energy transferred due to the cells only. At this point, the thermal mass is a composite of several values.

$$C_{th,total} = C_{th,cells} + C_{th,medium} + C_{th,DSC} \tag{6.3}$$

where $C_{th,total}$ is the total thermal mass of the system, $C_{th,cells}$ is the thermal mass of the cellular samples, $C_{th,medium}$ is the thermal mass of the cellular culture medium, and $C_{th,DSC}$ is the thermal mass of the DSC device.

To overcome this obstacle the differential of the response of the cells against the reference will be examined in the same process as was previously presented. By utilizing the differential of the sample versus the reference we can eliminate the contribution of thermal mass of the DSC device. We can further isolate the cellular response by subtracting the differential buffer medium data from the differential cellular data. This way we can eliminate the contribution of the thermal masses due to the cell culture medium.

6.2 Derivative Method Two, Differential

For the second method, the differential of the cellular sample from the reference medium will be plotted and fitted in the same fashion as previously presented. This will isolate the response to that of only the cellular sample. From there, a comparison of the derivative will be presented.

The differential from the experiments performed using the JM-1 liver cancer cell line is shown in figure 6.2-1 with the fit overlaid.

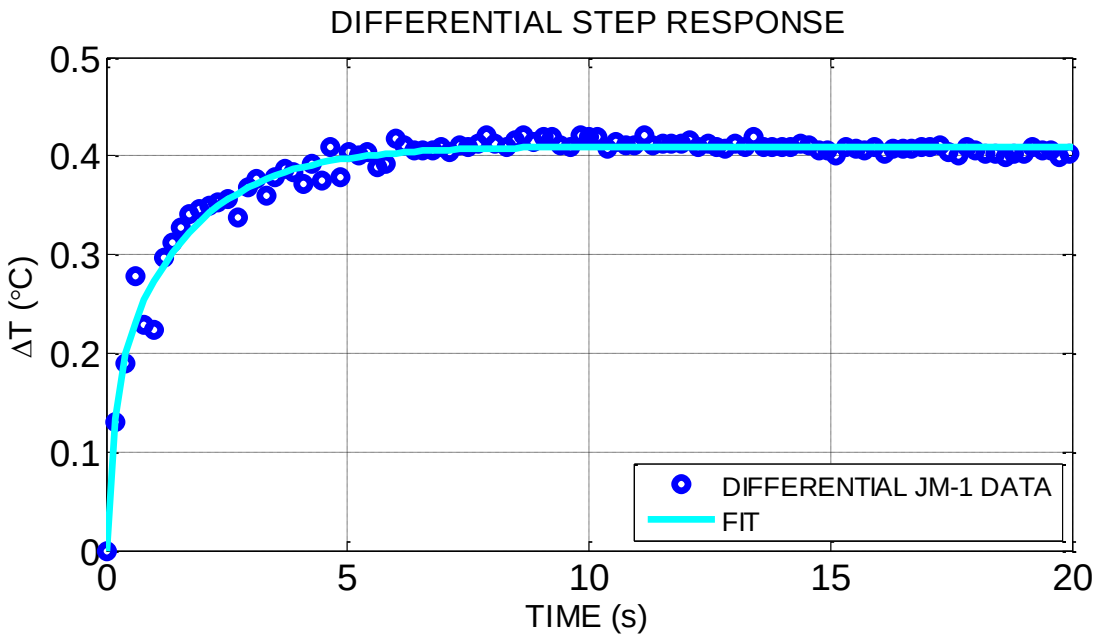

Figure 6.2-1. Differential heating response of JM-1 cells. Exponential fitting overlaid.

Using MATLAB's curve fitting toolbox, the first derivative is obtained, $\frac{d\Delta T}{dt}$ and plotted versus time, figure 6.2-2. Next, the differential data from the experiments done with the lymphocytes is examined; again, the data is corrected and fitted using the same function. The step response is shown in figure 6.2-3.

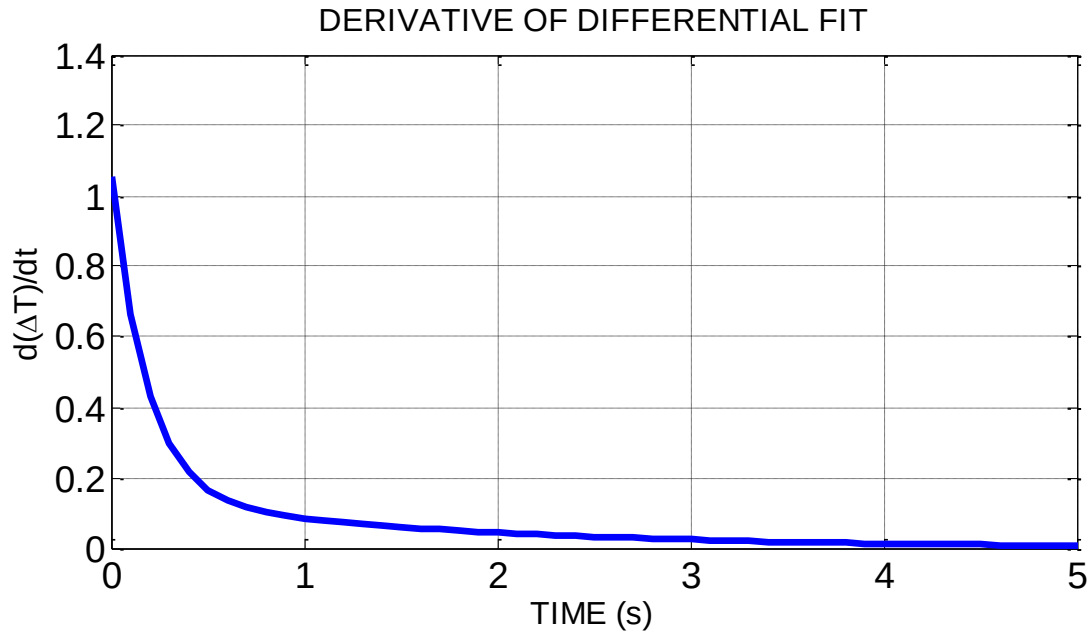

Figure 6.2-2. First derivative of the differential heating response of JM-1 cells.

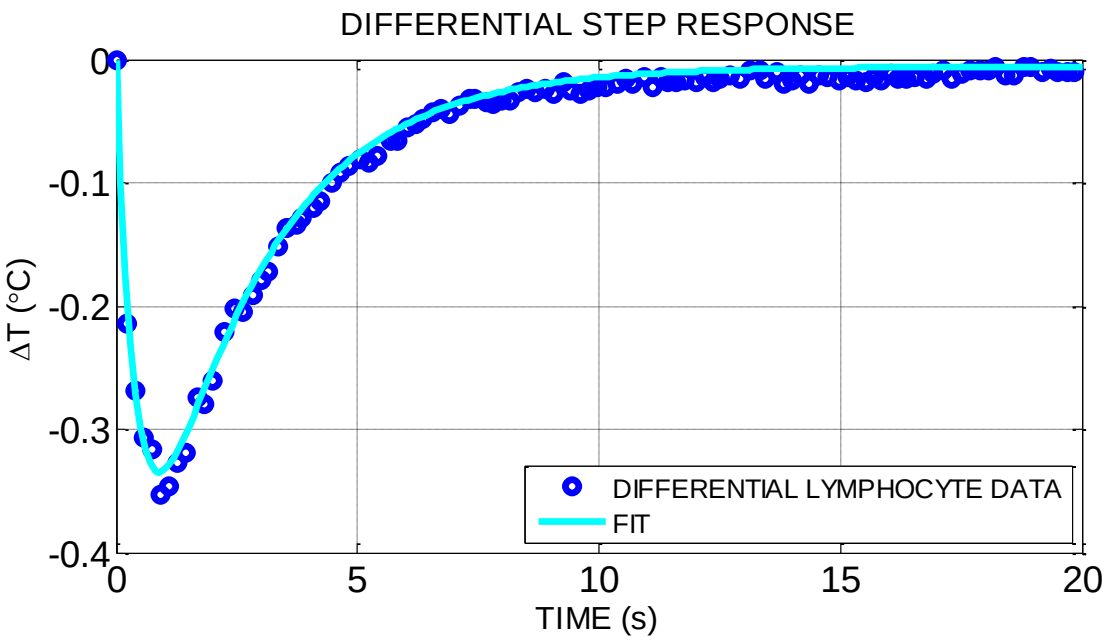

Figure 6.2-3. Differential heating response of lymphocytes. Exponential fitting overlaid.

Using MATLAB's curve fitting toolbox, the first derivative is obtained, $\frac{d\Delta T}{dt}$, and plotted versus time, figure 6.2-4.

The coefficients for the fitting of the differential responses shown in figure 6.2-1 and 6.2-3 are given in the following table:

Differential Step Response	a	b	c	d
JM-1	0.162	5.69	0.2476	0.6054
Lymphocytes	0.579	0.42	-0.5849	2.393

Table 6.2-1. Coefficients for fitting equation.

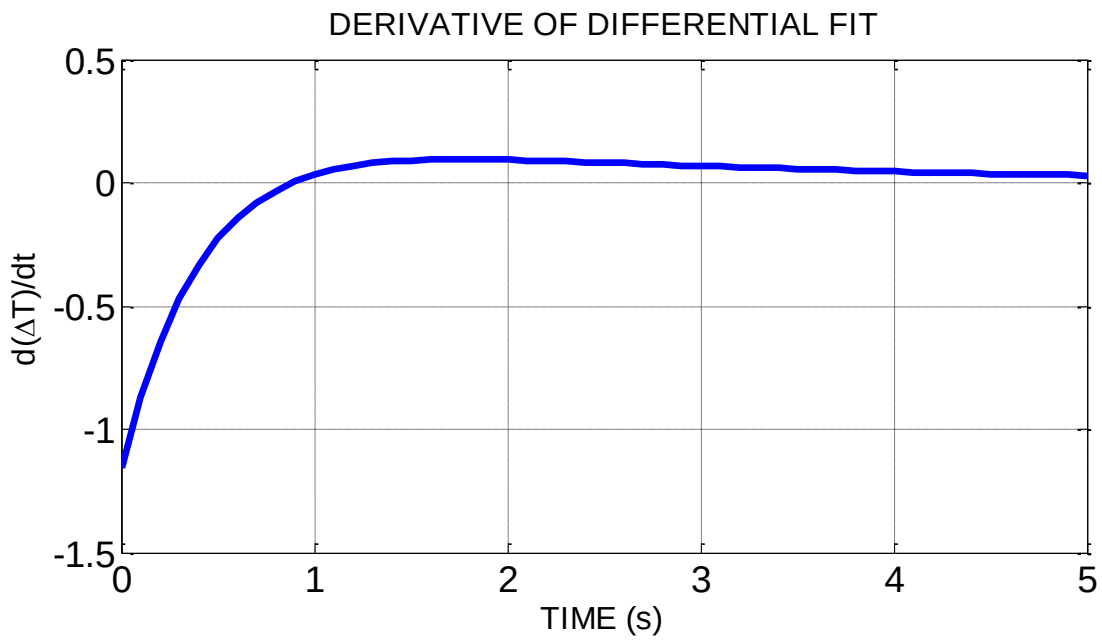

Figure 6.2-4. First derivative of the differential heating response of lymphocytes.

Now we compare the results from this method of post processing analysis. As seen in figure 6.2-5, there is still a noticeable difference in the response of the cell types, which allows the ability to distinguish between them. There is now the opportunity to extract the heating rate of the cells because the thermal mass contributions from the medium and DSC have been eliminated.

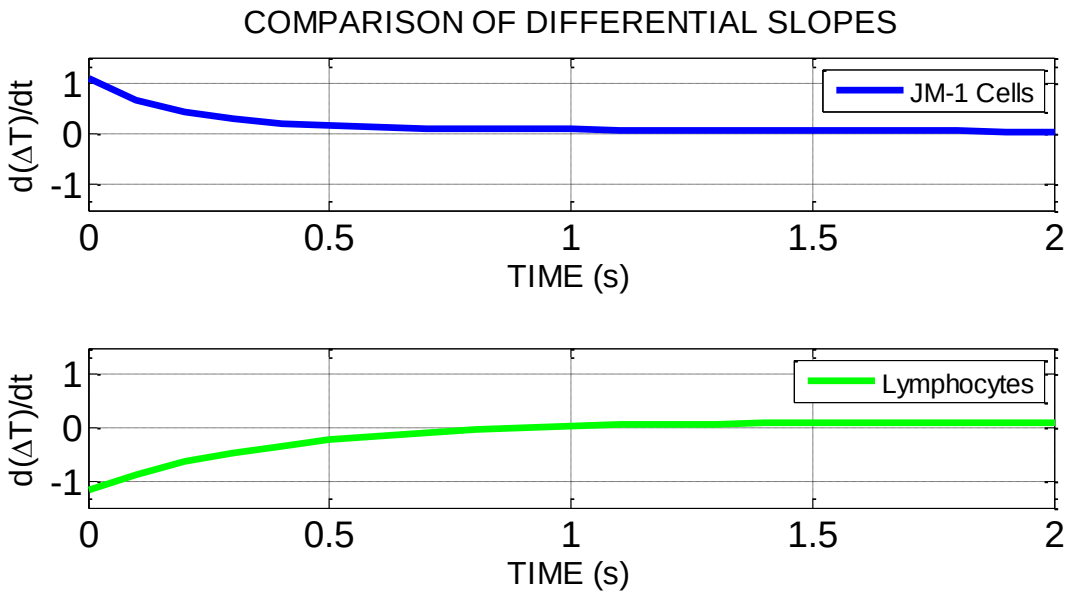

Figure 6.2-5. Derivative Comparison of the slopes of the temperature curves for JM-1 cells and lymphocytes.

6.3 Cellular Heating Rate

Next the cellular heating rate will be obtained from the DSC data. The heating rates of the cells give insight into the condition of the cells metabolism rate. The misregulation of cell physiology due to diseases and cancers advances the metabolism and they often have an increase heat output. Along with distinguishing between cells by obtaining the derivative of the DSC curve, information like the heating rate allows for an additional means to identify cells in a population.

In order to extract the heating rate of the cells we first must extract the value of thermal capacitance for each cell type. The thermal capacitance is related to the slope of the step response and the applied power by the following relationship.

$$C_{th} = P_{in} \cdot \left[\left. \frac{d\Delta T}{dt} \right|_{t=0} \right]^{-1} \tag{6.4}$$

where C_{th} is thermal mass, P_{in} is the applied input power, and $\left. \frac{d\Delta T}{dt} \right|_{t=0}$ is the value of the slope of the differential step response at zero.

Cell type	Pin (J/s)	$\left. \frac{d\Delta T}{dt} \right|_{t=0} \left(^{o}\mathrm{C/s}\right)$	Cth (J/^{o}C)
JM-1 Liver cells	0.012723	1.057	0.012037334
Lymphocytes	0.005413	-1.268	-0.004678178

Table 6.3-1. Determination of thermal capacitance.

Once the thermal capacitance is obtained, we can gather information about the heat transfer through the following relationship.

$$Q = C_{th} \cdot \Delta T \tag{6.5}$$

Plotting Q versus time from equation four and using the absolute value of thermal capacitance along with the data values from the applied step responses we can obtain the heat transferred from the two cell types. Figures 6.3-1 & 6.3-2 show the results.

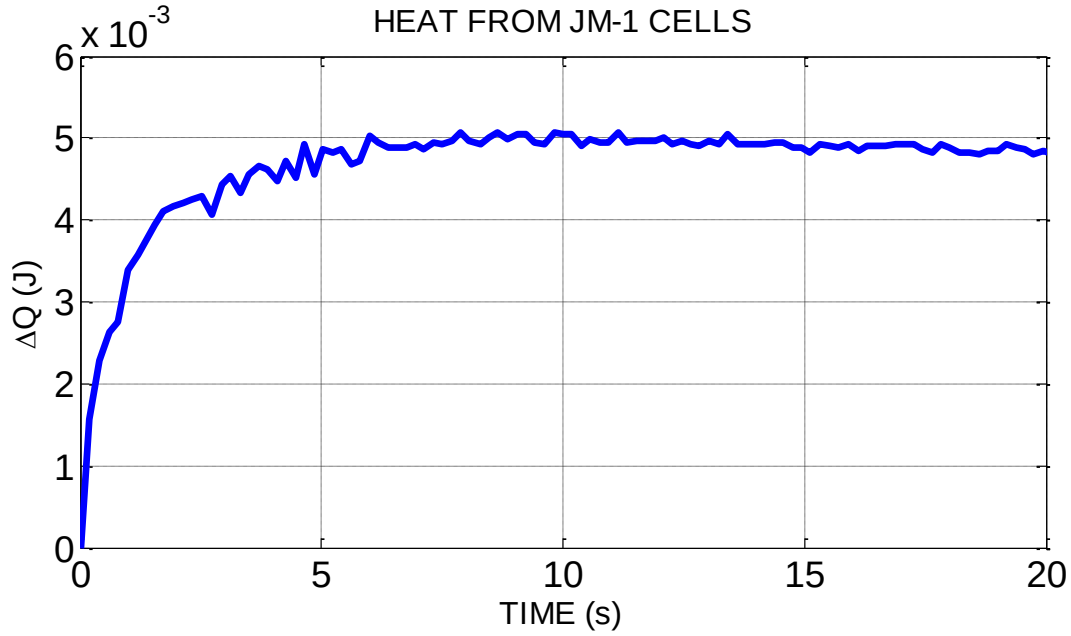

Figure 6.3-1. Heat transferred due to JM-1 cells.

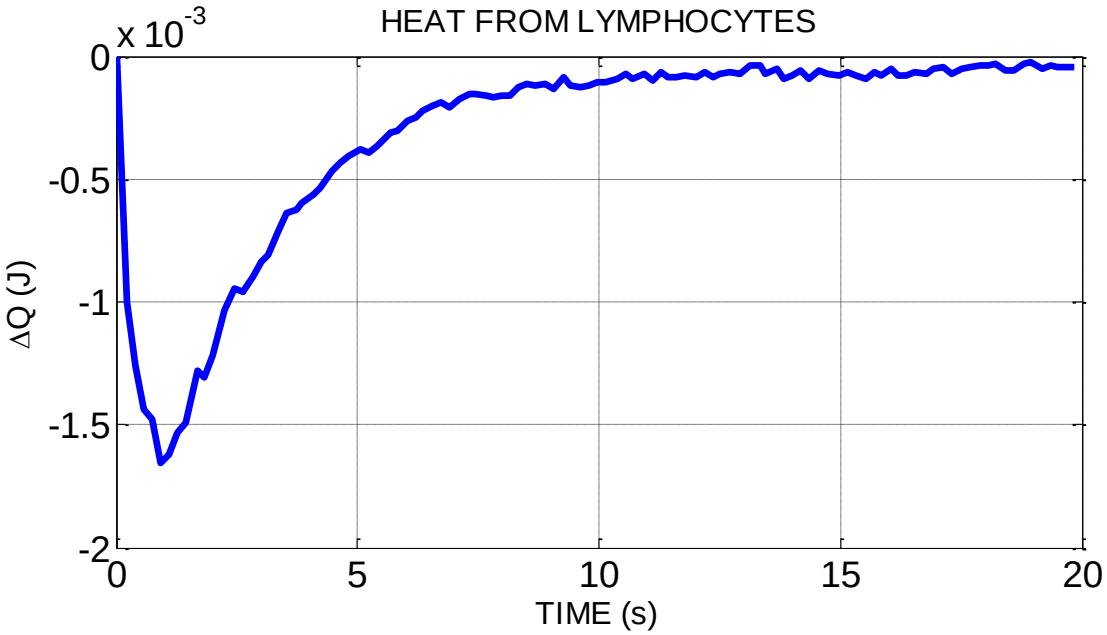

Figure 6.3-2. Heat transferred due to lymphocytes.

If we take the derivative of these plots in the same fashion as presented earlier, we can obtain the heat transfer rates of the two cell types. Figure 6.3-3 shows the results of the curve fitting and derivative analysis for both cells.

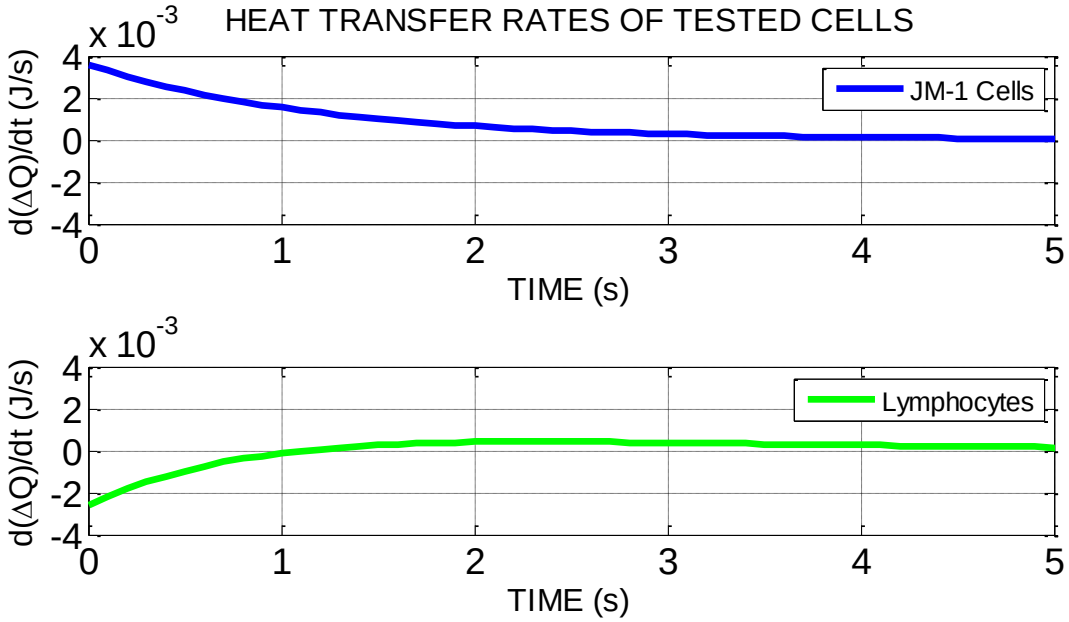

Figure 6.3-3. Heating rates for both tested cell lines.

As figure 6.3-3 shows, the rate of heat transferred from the JM-1 cells is positive, which supports the theory that the cells are adding their thermal energy to increase the temperature of the sample chamber as compared to the reference chamber. As for the lymphocytes, their rate is negative, suggesting that they are absorbing the thermal energy that is being put into the system from the applied step input. These results also support the initial data results showing that the sample and reference were approximately equal in their temperature response. The decaying nature of the curves is due to the fact that as the chambers begin to reach steady state the rates of heat transfer approach zero.

6.4 Discussion

After the initial testing was completed, it was shown that the JM-1 liver cancer cells had increased the temperature of the sample chamber compared to the reference chamber, while no distinguishable difference was observed with the lymphocytes. That proved inconclusive as a means to distinguish between the two cells. Therefore, additional post processing techniques were used to attempt to improve the ability to identify the cells and determine their thermal energy contributions. By obtaining the derivative of both the raw sample and differential sample ΔT curves, we have shown that it is possible to distinguish between the two cells. The differential method proves advantageous over the direct method as it isolates the response to that of only the cells by eliminating any internal device and external environmental effects. Further it allows determining information about the heat transfer due to the cells. It was shown that JM-1 liver cancer cells initially have a positive heat transfer rate and generate approximately 5mW of thermal energy due to their increased metabolism. Although this result seems high, very high densities of cells were used to perform the experiments from 20000 per µl to 10^6 per µl. Heat rates for single cells range from 330pW to 100nW[25]. In contrast, lymphocytes initially have a negative heat transfer rate and absorb thermal energy. These rates both then decay to zero as the system reaches steady state.

7 Conclusion

This chapter will summarize the thesis by reviewing the design, fabrication, characterization and experimental measurements performed. Results obtained from the experimental measurements will also be reviewed. Suggestions for additional work and improvements to the DSC will be presented.

7.1 Summary

This thesis presented a micromachined differential scanning calorimeter (DSC) for cellular differentiation and metabolism monitoring. Chapter 1 presented the motivation for the development of the DSC and its intended application. Chapter 2 discussed the design requirements. Chapter 3 detailed the fabrication processes involved in producing the physical device. Chapter 4 covered the device calibration and characterization to determine the performance and operating specifications. Chapter 5 discussed the procedures and initial results of cellular metabolism experiments. Chapter 6 presented the analysis of the results obtained from the metabolism monitoring experiments.

7.2 Conclusions

The goal of this thesis work was to observe measure and quantify the heat generated by the metabolism of biological cells using a micromachined calorimeter. The cell is the fundamental building block of all multi-cellular organisms. The misregulation of cell physiology due to disease increases the metabolic rate of the cell and therefore its

heat output. By observing or monitoring the cell's heat output will lead to a method to detect diseased cells and distinguish them from normal cells.

Micro-calorimetry is a very useful technique in the biological sciences for the study of the energy generation and metabolism monitoring. These devices can achieve excellent thermal isolation by using nitride-based membranes as support structures, and very sensitive sensors through thin film resistive temperature detectors. The fabricated DSC uses twin calorimetric chambers with nickel resistive temperature detectors and integrated nickel resistive heaters to apply on chip heating and calibration. The chambers are formed by a backside etch process that produces a 500nm thick nitride film on the front side where the sensors and heaters are fabricated. Sample and reference materials are manually loaded from the back.

The cell metabolism experiments carried out with the DSC were done using JM-1 liver cancer cells and white blood cells (lymphocytes). Step voltage inputs were applied to the DSC while the response of the RTD temperature was monitored. The results from initial testing show a detectable increase in chamber temperature of 0.375ºC for the JM-1 liver cells, while results from testing lymphocytes proved to be inconclusive. Further analysis was done by obtaining the derivative of the DSC temperature curves. Two methods were explored, the direct derivative of the raw data curve and the derivative of the differential data curve. While both methods proved the ability to differentiate between the JM-1 liver cells and the lymphocytes, the derivative of the differential was superior due to the elimination of common mode signals. The differential method also allowed the determination of the heat output and heat rates of the cells. JM-1 liver cells showed a heat output of approximately 5mW and a positive heat rate, which is consistent with its

increased metabolism, while the lymphocytes showed a negative heat rate or absorption of 1.5mW of thermal energy.

Although these suggested rates are high, the density of cells used in the experiments ranged from 20000 per µl to 10^6 per µl. This high density may drive the value of the heat contribution away from the actual value that is produced by the cells. With further improvements to the device, lower cell densities can be used and a more accurate determination of the cellular heating rate can be obtained.

7.3 Future Work

What follows is a list of suggested changes to the DSC to improve its performance for cellular metabolism monitoring, and some suggestions for performing the experiments.

Increase the length or number of RTD traces to improve the base resistance will help to improve the sensitivity. Also, increasing the heater length will improve the temperature uniformity. Reducing the RTD trace width to less the 5µm will significantly improve the sensitivity. If the supporting membrane was made larger, or a three dimensional chamber was designed from the nitride film, the thermal isolation and thermal mass could be greatly improved, which would reduce the thermal equilibrium time constant. Separation of the sample and reference chambers by a greater distance will reduce the crosstalk.

Cellular experiments should be performed as quickly as possible to reduce the oxygen consumption by the cells, which increases the chance for cell death. When

setting up experiments, buffer-only tests are important to determine the correct value of voltage to be applied to ensure 37ºC. Although37ºC logically seems like the optimal temperature to perform experiments, results may be improved at a slightly lower or higher temperature. Therefore, a range of temperatures should be evaluated for a given cell type.

If the sensitivity is improved, it should be possible to determine the minimum cell count to observe a detectable signal. The goal for a cell number should be progressively driven down to 1000, 100, or even 10 cells to achieve an accurate value of the particular cell's heat rate.

8 Bibliography

[1]. Kwak, B.S., et al. "Dual Thermopile Integrated Microfluidic Calorimeter for Biochemical Thermodynamics." Microfluid Nanofluid 5 (2008): 255-262.

[2]. Lerchner, J., et al. "A New Micro-fluid Chip Calorimeter for Biochemical Applications." Thermochimica Acta 445 (2006): 144-150.

[3]. Xu, Junkai. Nanocalorimetric Sensor for Ultra-Low-Volume Biological Measurements and Calibration by Chemical Method. PhD Thesis. Ann Arbor: ProQuest LLC, 2007.

[4]. Johannessen, Erik, et al. "Micromachined Nanocalorimetric Sensor for Ulta-Low-Volume Cell-Based Assays." Anal. Chem. 74 (2002): 2190-2197.

[5]. Verhaegen, Katarina, et al. "A High-throughput Silicon Microphysiometer." Sensors and Actuators 82 (2000): 186-190.

[6]. Price, A. and C. Culbertson. "Chemical Analysis of Single Mammalian Cells with Microfluidics." American Chemical Society 7 April 2007: 2615-2621.

[7]. Zhang, Yuyan. A Micromachined Thermal Sensor for Biochemical Sensing and Polymer Characterization. PhD Thesis. Ann Arbor, Mi: ProQuest, 2005.

[8]. DeBusschere, B.D. Portable Cell-Based Biosensors. PhD Thesis. Ann Arbor, MI: ProQuest LLC, 2002.

[9]. Cooper, G. and R. Hausman. The Cell: A Molecular Approach. Washington, D.C.: ASM Press, 2007.

[10]. Karp, G. Cell and Molecular Biology. Hoboken: Wiley, 2010.

[11]. Haines, P.J. "Introduction." Haines, P.J. Principles of Thermal Analysis and Calorimetry. Cambridge, UK: The Royal Society of Chemisry, 2002.

[12]. Hemminger, W. and G. Hohne. Calorimetry: Fundamentals and Practice. Deerfield Beach: Weinheim, 1984.

[13]. Hohne, G.W., W.F. Hemminger and H.-J. Flammersheim. Differential Scanning Calorimetry. Berlin: Springer, 2003.

[14]. Willson, R.J. "Calorimetry." Haines, J.P. Principles of Thermal Analysis and Calorimetry. Cambridge, UK: The Royal Society of Chemistry, 2002. 129-161.

[15]. Laye, P.G. "Differential Thermal Analysis and Differential Scanning Calorimetry." Haines, J.P. Principles of Thermal Analysis and Calorimetry. Cambridge, UK: The Royal Society of Chemistry, 2002. 55-92.

[16]. Fraden, J. Handbook of Modern Sensors. New York: Springer, 2000.

[17]. Carstens, J. Electrical Sensor and Transducers. Upper Saddle River: Regents/Prentice Hall, 1993.

[18]. Hsu, T.-R. MEMS and Microsystems. Hoboken: Wiley, 2008.

[19]. Wilson, J. and A. Buffa. College Physics. Upper Saddle River: Prentice Hall, 2003.

[20]. Norton, H. Handbook of Transducers. Englewood Cliffs: Prentice Hall, 1989.

[21]. Shackelford, J. Introduction to Materials Science for Engineers. Prentice Hall, 1995.

[22]. Smith, W. and J. Hashemi. Foundations of Materials Science and Engineering. New York: McGraw-Hill, 2006.

[23]. Madou, M. Fundamentals of Microfabrication. Boca Raton: CRC Press, 1997.

[24]. Baliga, R. Thermal and Electrical Characterization of a Micro-Hotplate for Calorimetry. Masters Thesis. Ann Arbor: ProQuest, 2004.

[25]. Lerchner, J., T. Maskow and G. Wolf. "Chip Calorimetry and its use for Biochemical and Cell Biological Investigations." Chemical Engineering and Processing (2008): 991-999.

Additional Supportive Material

Bousse, L. "Biosensors with Microvolume Reaction Chambers." Yamauchi, S. Chemical Sensor Technology. Tokyo: Kodansha, 1988.

Cooper, G. and R. Hausman. The Cell: A Molecular Approach. Washington, D.C.: ASM Press, 2007.

Edleman, P. and J. Wang. Biosensors & Chemical Sensors: Optimizing Performance Through Polymeric Materials. Washington, D.C.: American Chemical Society, 1992.

Lee, J., et al. "Differential Scanning Calorimeter Based on Suspended Membrane Single Crystal Silicon Microhotplate." Journal of Microelectromechanical Systems (2008): 1513-1525.

Lee, W., et al. "High-Sensitivity Microfluidic Calorimeters for Biological and Chemical Applications." PNAS (2009): 15225-15230.

Lerchner, J., et al. "Nano-Calorimetry of Small-Sized Biological Samples." Thermochimica Acta (2008): 48-53.

McClain, M., et al. "Microfluidic Devices for the High-Throughput Chemical Analysis of Cells." Anal. Chem. (2003): 5646-5655.

Sedgwick, H., et al. "Lab-on-a-Chip Technologies for Proteomic Analysis from Isolated Cells." J. R. Soc. Interface (2008): S123-S130.

Toriello, N.M., et al. "Integrated Microfluidic Bioprocessor for Single-Cell Gene Expression Analysis." PNAS 105.51 (2008): 20173-20178.

Wheeler, A., et al. "Microfluidic Device for Single-Cell Analysis." Anal. Chem. (2003): 3581-3586.

Wilson, J,. "Sensor Technology Handbook." Lee, Y. and R. Hausman. Biosensors. Amsterdam: Elsevier, 2005. 161-179.

Wlodkowic, D., et al. "Microfluidic Single-Cell Array Cytometry for the Analysis of Tumor Apoptosis." Anal. Chem. (2009): 5517-5523.

Xu, J., et al. "A Microfabricated Nanocalorimeter: Design, Characterization, and Chemical Calibration." Anal. Chem. (2008): 2728-2733.

Xu, Y., et al. "Aptamer-Based Microfluidic Device for Enrichment, Sorting, and Detection of Multiple Cancer Cells." Anal. Chem. (2009): 7436-7442.

Zhang, Y, and S, Tadigadapa. "Calorimetric Biosensors with Integrated Microfluidic Channels." Biosensors & Bioelectronics (2004): 1733-1743.

Zhang, Y. and S, Tadigadapa. "Microthermopiles Integrated with Fluidic Channels as Calorimeteric MEMS Biosensors." The 12th International Conference on Solid State Sensors, Actuators and Microsystems. Boston: IEEE, 2003. 1176-1179.